

**DETERMINATION OF STRESS VS. TEMPERATURE
PHASE DIAGRAM OF NITI SHAPE MEMORY ALLOYS
WITH DIFFERENT POROSITY LEVELS**

**FARKLI GÖZENEK ORANLARINA SAHİP NİTİ ŞEKİL
BELLEK ALAŞIMLARININ GERİLİM-SICAKLIK FAZ
DİAGRAMLARININ BELİRLENMESİ**

GÜLFEM İNANER

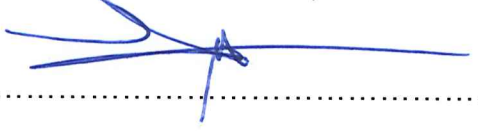
ASSOC. PROF. DR. BENAT KOÇKAR
Supervisor

Submitted to Graduate School of Science and Engineering of Hacettepe University
as a Partial Fulfilment to the Requirements
for the Award of the Degree of Master of Science
in Mechanical Engineering

2018

This work named "**Determination of Stress vs. Temperature Phase Diagram of NiTi Shape Memory Alloys with Different Porosity Levels**" by GÜLFEM İNANER has been approved as a thesis for the Degree of **MASTER OF SCIENCE IN MECHANICAL ENGINEERING** by the below mentioned Examining Committee Members.

Assoc. Prof. Dr. Bora Maviş
Head



.....

Assoc. Prof. Dr. Benat KOÇKAR
Supervisor



.....

Assoc. Prof. Dr. Zarife Göknur Büke
Member



.....

Assist. Prof. Dr. Bilsay Sümer
Member



.....

Assist. Prof. Dr. Okan Görtan
Member



.....

This thesis has been approved as a thesis for the Degree of **MASTER OF SCIENCE IN MECHANICAL ENGINEERING** by Board of Directors of the Institute for Graduate School of Science and Engineering.

Prof. Dr. Menemşe GÜMÜŞDERELİOĞLU
Director of the Institute of
Graduate School of Science and Engineering

YAYINLAMA VE FİKRİ MÜLKİYET HAKLARI BEYANI


Enstitü tarafından onaylanan lisansüstü tezimin / raporunun tamamını veya herhangi bir kısmını, basılı (kağıt) ve elektronik formatta arşivleme ve aşağıda verilen koşullarla kullanıma açma iznini Hacettepe Üniversitesine verdiğimi bildiririm. Bu izinle Üniversiteye verilen kullanım hakları dışındaki tüm fikri mülkiyet haklarım bende kalacak, tezimin tamamının ya da bir bölümünün gelecekteki çalışmalarda (makale, kitap, lisans ve patent vb.) kullanım hakları bana ait olacaktır.

Tezin kendi orijinal çalışmam olduğunu, başkalarının haklarını ihlal etmediğimi ve tezimin tek yetkili sahibi olduğumu beyan ve taahhüt ederim. Tezimde yer alan telif hakkı bulunan ve sahiplerinden yazılı izin alınarak kullanılması zorunlu metinlerin yazılı izin alınarak kullandığımı ve istenildiğinde suretlerini Üniversiteye teslim etmeyi taahhüt ederim.

Yükseköğretim Kurulu tarafından yayınlanan “Lisansüstü Tezlerin Elektronik Ortamda Toplanması, Düzenlenmesi ve Erişime Açılmasına İlişkin Yönerge” kapsamında tezim aşağıda belirtilen koşullar haricinde YÖK Ulusal Tez Merkezi / H. Ü. Kütüphaneleri Açık Erişim Sisteminde erişime açılır.

- o Enstitü / Fakülte yönetim kurulu kararı ile tezimin erişime açılması mezuniyet tarihimden itibaren 2 yıl ertelenmiştir. ⁽¹⁾
- o Enstitü / Fakülte yönetim kurulunun gerekçeli kararı ile tezimin erişime açılması mezuniyet tarihimden itibaren Ay ertelenmiştir. ⁽²⁾
- o Tezimle ilgili gizlilik kararı verilmiştir. ⁽³⁾

18/09/2018


Gülfem İnaner

“Lisansüstü Tezlerin Elektronik Ortamda Toplanması, Düzenlenmesi ve Erişime Açılmasına İlişkin Yönerge”

- (1) Madde 6. 1. Lisansüstü teze ilgili patent başvurusu yapılması veya patent alma sürecinin devam etmesi durumunda, tez danışmanının önerisi ve enstitü anabilim dalının uygun görüşü üzerine enstitü veya fakülte yönetim kurulu iki yıl süre ile tezin erişime açılmasının ertelenmesine karar verebilir
- (2) Madde 6. 2. Yeni teknik, materyal ve metotların kullanıldığı, henüz makaleye dönüşmemiş veya patent gibi yöntemlerle korunmamış ve internetten paylaşılması durumunda 3. Şahıslara veya kurumlara haksız kazanç imkanı oluşturabilecek bilgi ve bulguları içeren tezler hakkında tez danışmanının önerisi ve enstitü anabilim dalının uygun görüşü üzerine enstitü ve fakülte yönetim kurulunun gerekçeli kararı ile altı ayı aşmamak üzere tezin erişime açılması engellenebilir.
- (3) Madde 7. 1. Ulusal çıkarları veya güvenliği ilgilendiren, emniyet, istihbarat, savunma ve güvenlik, sağlık vb. konulara ilişkin lisansüstü tezlerle ilgili gizlilik kararı, tezin yapıldığı kurum tarafından verilir*. Kurum ve kuruluşlarla yapılan işbirliği protokolü çerçevesinde hazırlanan lisansüstü tezlere ilişkin gizlilik kararı ise, ilgili kurum ve kuruluşun önerisi ile enstitü veya fakültenin uygun görüşü üzerine üniversite yönetim kurulu tarafından verilir. Gizlilik kararı verilen tezler Yükseköğretim Kuruluna bildirilir.
Madde 7. 2. Gizlilik kararı verilen tezler gizlilik süresince enstitü veya fakülte tarafından gizlilik kuralları çerçevesinde muhafaza edilir, gizlilik kararının kaldırılması halinde Tez Otomasyon Sistemine yüklenir.

* Tez danışmanının önerisi ve enstitü anabilim dalının uygun görüşü üzerine enstitü veya fakülte yönetim kurulu tarafından karar verilir.



To my beloved sister...

ETHICS

In this thesis study, prepared in accordance with the spelling rules of Institute of Graduate Studies in Science of Hacettepe University,

I declare that

- all the information and documents have been obtained in the base of the academic rules
- all audio-visual and written information and results have been presented according to the rules of scientific ethics
- in case of using others Works, related studies have been cited in accordance with the scientific standards
- all cited studies have been fully referenced
- I did not do any distortion in the data set
- and any part of this thesis has not been presented as another thesis study at this or any other university.

18/09/2018



GÜLFEM İNANER

ABSTRACT

DETERMINATION OF STRESS VS. TEMPERATURE PHASE DIAGRAM OF NITI SHAPE MEMORY ALLOYS WITH DIFFERENT POROSITY LEVELS

İnaner, Gülfem

Master of Science, Department of Mechanical Engineering

Supervisor: Assoc. Prof. Benat Koçkar

September 2018

Having many superior properties compared to conventional materials, shape memory alloys (SMAs) have been studied and used in many engineering applications over the last four decades. As one of the commonly used SMAs, NiTi alloys also distinguish from Cu-based and Fe-based SMAs with their large recoverable strains, biocompatibility, and thermo-mechanical performance which make them promising materials in aerospace, biomedical and other commercial applications. Beside these properties, porous NiTi alloys also provide lower density with high stiffness, higher gas permeability and better biomechanical compatibility due to its Young's Modulus which is similar to bones. In spite of these advanced properties, thermo-mechanical behavior of porous NiTi alloys has not been well-known yet.

In this study, stress vs temperature phase diagram and super-elasticity behavior of porous Ni-rich NiTi alloys with different porosity levels including 10%, 20%, 30% and 40% by volume were determined by microstructural, thermal and mechanical characterizations tests. Porous specimens with 10 mm diameter were produced from NiTi and Mg powders with hydraulic pressing and conventional sintering. The porosity in these specimens was formed by space holder technique with magnesium powder particles. The porosity levels and porosity architecture of specimens were validated via using Optical Microscope (OM). The thermal characterization of the porous alloys was done by DSC analysis to determine the phase transformation temperatures (M_s , M_f , A_s and A_f) of the samples. The superelasticity experiments with the application of compressive force to these specimens were conducted for the determination of the M_d point. M_d point is defined as the highest temperature at which stress induced martensite can be obtained by loading. Uniaxial compression tests performed at different temperatures starting from $M_s+15^\circ\text{C}$ by loading up to 3% constant strain value was achieved and unloading to 0 MPa level. The temperature of the specimen was increased by 30°C in each cycle till the reverse transformation was vanished. After these procedures, the phase diagrams of Ni-rich NiTi alloys with different porosity levels were obtained in order to identify temperature window at which superelasticity was observed for novel actuator applications.

Keywords: Porous shape memory alloys, NiTi alloys, phase diagram, stress-induced martensite

ÖZ

FARKLI GÖZENEK ORANLARINA SAHİP NİTi ŞEKİL BELLEK ALAŞIMLARININ GERİLİM-SICAKLIK FAZ DİAGRAMLARININ BELİRLENMESİ

Gülfem İNANER

Yüksek Lisans, Makine Mühendisliği

Tez Danışmanı: Doç. Dr. Benat Koçkar

Eylül 2018

Konvansiyonel malzemelerle karşılaştırıldığında bir çok ayırt edici özelliğe sahip olan şekil bellek alaşımları son 40-50 yıldır çalışılmakta ve mühendislik uygulamalarında kullanılmaktadır. En çok kullanılan şekil bellek alaşımlarından olan NiTi alaşımları ise yüksek geri kazanılabilen gerinimi, biyo-uygunluğu, ve termomekanik performansı ile Cu-bazlı Fe-bazlı diğer şekil bellek alaşımlarından ayrılarak havacılık, biyomedikal ve diğer ticari uygulamalarda iyi bir yer edinmiştir. Bu özelliklerin yanında, gözenekli NiTi alaşımları ise düşük yoğunlukta yüksek mukavemet, gaz geçirebilirliği ve kemiğe yakın elastik modülüsü ile daha yüksek biyomekanik uygunluğa sahiptir. Bu ileri özelliklerine rağmen, gözenekli NiTi alaşımlarının termomekanik davranışları henüz çok iyi bilinmemektedir.

Bu çalışmada, farklı gözenek oranlarına (%10, %20, %30 ve %40 gözenekli) sahip NiTi alaşımlarının gerilim-sıcaklık faz diagramları ve super-elastik davranışları mikroyapısal, termal ve mekanik karakterizasyon testleri kullanılarak belirlenmiştir. 10 mm çapa sahip olan gözenekli numuneler NiTi ve Mg tozlarının hidrolik pres ile sıkıştırılması ve konvansiyonel sinterleme yöntemleri ile üretilmiştir.

Numunelerdeki gözenekli yapı magnezyum boşluk tutucu yöntemi kullanılarak elde edilmiştir. Mikroyapısal karakterizasyon testleri (optic mikroskop) ile numunelerin gerçek gözenek oranları ve yapıları teyit edilmiştir. Gözenekli numunelerin termal karakterizasyonu ise diferansiyel taramalı kalorimetre (DSC) analizi ile faz değişim sıcaklıklarının (M_s , M_f , A_s ve A_f) belirlenmesi yardımı ile yapılmıştır. Süper-elastik karakterizasyonu ise farklı sıcaklıklarda (%3 sabit gerinime kadar yüklenmesi $M_s+15^\circ\text{C}$ sıcaklıktan başlanarak her testte numune sıcaklığını 30°C artırılması ile) gerçekleştirilmiş olan basma testlerinde M_d sıcaklığının (gerilim sebepli martensit fazing görüldüğü en yüksek sıcaklık) belirlenmesi ile yapılmıştır. Bu prosedürlerden sonra, farklı gözenek oranlarına sahip Ni-zengin NiTi alaşımlarının faz diagramları, yeni mühendislik uygulamaları için akma mukavemetinin sıcaklık ile yükseldiği sıcaklık aralığını (M_s ve M_d arasında) belirlemek için oluşturulmuştur.

Anahtar Kelimeler: Gözenekli şekil bellek alaşımları, NiTi alaşımlar, faz diagramı, gerilim sebepli martensit

ACKNOWLEDGEMENTS

This thesis would not have been possible without the support of many people. I wish to express my deepest appreciation to my supervisor, Assoc. Prof. Dr. Benat Koçkar. This thesis would not be possible without her support and guidance. Many thanks also go to my committee members for their time, insightful comments and constructive criticism for my study.

I would also give thanks to my laboratory mates Halil Onat Tuğrul, Şule Çakmak and Hasan Hüseyin Saygılı for their support and friendship, they helped me to overcome many problems that I encountered during experiments.

I am especially grateful to Beril Aba, Alişan Balkoca, Ezgi Erdoğan and Beybin İlhan for their endless support, encouragement and love; their presence always reminded me how lucky I am to have them. I am also thankful to my dearest friends; Cemre Artan, Ahmet Fatih Koç, Cankat Ayas, Gülin Başkes,, Didem Gül, Sezin Köseoğlu, Nağme Kaşmer and Esmeray Üstünyağız for their valuable friendship and all the greatest times we have spent together.

Last but not least, I would also like to acknowledge the generous support of my family Gülru İnaner İşli, Elfide İnaner, Hikmet İnaner and my aunt Hülya İnaner during completion of this study.

TABLE OF CONTENT

ABSTRACT	i
ÖZ	iii
ACKNOWLEDGEMENTS.....	v
TABLE OF CONTENT	vi
LIST OF TABLES	ix
LIST OF FIGURES.....	x
LIST OF SYMBOLS AND ABBREVIATIONS	xiii
1. INTRODUCTION.....	1
1.1. State of the Art.....	1
1.1.1 Shape Memory Effect & Superelasticity	1
1.1.2 Ni-Ti Shape Memory Alloys.....	3
1.1.3 Ni-Ti Alloys with Porosity and Their Characterization in Literature.....	7
1.2. Objective	9
1.3. Expected Impact.....	9
2. LITERATURE REVIEW	11
2.1. Production of Porous NiTi Alloys	11
2.1.1 Existing Porous NiTi Production Methodologies.....	11
2.1.2 Powder Metallurgy Techniques used for Porosity Formation	11
2.1.3 Space Holder Technique and Magnesium	15
2.2. Superelasticity Characterization	16
2.2.1 Maximum Temperature to Induce Martensite (M_d)	16
2.2.2 Superelasticity Behaviour of Porous NiTi Alloys Produced with SPT	18
3. EXPERIMENTAL PROCEDURE.....	20
3.1. Production of Specimens.....	21
3.1.1 Materials Used	21

3.1.2	Hydraulic Pressing	22
3.1.3	Two-step Conventional Sintering	23
3.2.	Macro-porosity Calculations	26
3.3.	Metallographic Imaging	28
3.4.	Differential Scanning Calorimeter Analysis.....	28
3.4.1	Specimen Preparation.....	29
3.4.2	DSC Analysis Procedure.....	29
3.5.	Superelasticity Tests	30
4.	RESULTS & DISCUSSION	33
4.1.	Production Process Review.....	33
4.2.	Thermal Characterization	39
4.3.	Structural Characterization of Specimens Produced	42
4.3.1	Porosity Levels and Distribution	42
4.3.2	Micrographs of the Specimens.....	43
4.4.	The Superelasticity Behaviour of Specimens	45
4.4.1	Superelasticity Behaviour with Temperature	46
4.4.2	Critical Stress to Induce Martensite vs Temperature Diagrams	54
4.4.3	Comparison of Young's Modulus and Irrecoverable Strain Amounts	57
5.	CONCLUSION	60
	REFERENCES.....	61
	APPENDIX 1: Technical Drawing of the Specimen Holder	64
	APPENDIX 2: Calculated Porosity Percentages by Image Analysis	65
	APPENDIX 3: Microscope Images of First 10% Mg Added Specimen	67
	APPENDIX 4: Microscope Images of First 20% Mg Added Specimen	69
	APPENDIX 5: Microscope Images of First 30% Mg Added Specimen	71
	APPENDIX 5: Microscope Images of First 40% Mg Added Specimen	73



LIST OF TABLES

Table 1 Some examples on characterization of porous NiTi alloys from literature .	7
Table 2 Comparison of porous NiTi production methodologies and common problems.....	14
Table 3 Formation energy of magnesium, nickel and titanium compounds in the working temperatures [8].....	16
Table 4 Estimated material amounts for porous NiTi.....	21
Table 5 Amounts of material used in specimens.....	33
Table 6 Comparison of the production processes of some specimens	35
Table 7 Digital Images of the produced specimens.....	36
Table 8 Phase transformation temperatures of specimens.....	40
Table 9 Macro-porosity amounts of specimens.....	43
Table 10 Compression Tests Temperature Levels for Every Specimen.....	45

LIST OF FIGURES

Figure 1 Phase transformation and twinning structure during shape memory behavior [3].....	1
Figure 2 A representative of stress-strain curve of superelastic material [4]	2
Figure 3 Nickel - Titanium Equilibrium Diagram[4]	4
Figure 4 Comparison between theoretical and experimental M_s temperature relation with Ni content in NiTi alloys [7].....	5
Figure 5 XRD results of NiTi alloy aged 1 hour at 400°C [8]	6
Figure 6 Illustration of SHS methodology [25]	12
Figure 7 Illustration of HIP methodology [30].....	13
Figure 8 Illustration of SPS methodology [16]	14
Figure 9 Representative Stress vs Temperature Phase Diagram of Shape Memory Alloys [34].....	17
Figure 10 Compression test results (RT) of 37% and 43% porous NiTi specimens with different production and aging processes from literature [8]	19
Figure 11 Compression test results (above A_f) of 37% and 43% porous NiTi specimens with different production and aging processes from literature [8]	19
Figure 12 Three parts of P/M mould and hydraulic pressing machine.....	23
Figure 13 Illustration of specimen holder set-up used during conventional sintering [8]	24
Figure 14 Ti6Al4V specimen holder	24
Figure 15 Conventional sintering furnace and high purity argon-filled tube.....	25
Figure 16 Grinder and polisher.....	26
Figure 17 Optical Microscope and the attached Camera	27
Figure 18 Example of the macro-porosity imaging of 10% porous specimen with Clemex Image Analysis software (a) image from the surface, (b) grey area scope used in image analysis calculations	28
Figure 19 Precision cutter used.....	29

Figure 20 Superelasticity test setup with extensometer	31
Figure 21 Compression test graphical user interface during a conducted test	32
Figure 22 Comparison of DSC heating and cooling curves of pre-alloyed NiTi specimens sintered 1 hour at 1100°C and 2 hours at 1200°C, with different porosity levels.....	40
Figure 23 Comparison of phase transformation temperature of specimens	41
Figure 24 Optical microscope images after grinding and polishing of (a) 10% porous specimen, (b) 20% porous specimen, (c) 30% porous specimen, (d) 40% porous specimen and (e) bulk specimen	42
Figure 25 Optical microscope images after etching of (a) 10% porous specimen (martensite exists at RT), (b) 20% porous specimen (martensite exists at RT), (c) 30% porous specimen (no martensite at RT), (d) 40% porous specimen (no martensite at RT) and (e) bulk specimen (no martensite at RT).....	44
Figure 26 Superelasticity behaviour of 20% porous specimen at 124°C, between Af and Md (selected for description).....	47
Figure 27 Stress-strain diagram of bulk specimen compressed to 3% strain level at different temperatures	48
Figure 28 Stress-strain diagram of 10% porous specimen compressed to 3% strain level at different temperatures	48
Figure 29 Stress-strain diagram of 20% porous specimen compressed to 3% strain level at different temperatures	49
Figure 30 Stress-strain diagram of 30% porous specimen compressed to 3% strain level at different temperatures	49
Figure 31 Stress-strain diagram of 40% porous specimen compressed to 3% strain level at different temperatures	50
Figure 32 Comparison of stress curves obtained by compression tests conducted at $M_s+75^\circ\text{C}$	52
Figure 33 Comparison of stress curves obtained by compression tests conducted at $M_s+355^\circ\text{C}$	53

Figure 34 Critical stresses to induce martensite of specimens at different test temperatures	54
Figure 35 Comparison of the mechanical behaviour of 20% porous specimen below and above M_d	55
Figure 36 Superelastic temperature window where superelasticity observed for every specimen	56
Figure 37 Comparison of phase transformation temperatures with M_d	57
Figure 38 Young's modulus comparison of specimens with respect to temperature	58
Figure 39 Irrecoverable strain amounts of specimens with respect to test temperatures	59

LIST OF SYMBOLS AND ABBREVIATIONS

Symbols

°	Degree
μ	Micro
σ	Stress
ε	Strain
E	Young's Modulus

Abbreviations

A _f	Austenite finish temperature
A _s	Austenite start temperature
CS	Conventional Sintering
DSC	Differential Scanning Calorimeter
HIP	Hot Isostatic Pressing
L	Length
LPS	Low Pressure Sintering
M _d	Maximum temperature martensite phase occurs
M _f	Martensite finish temperature
Mg	Magnesium
MIM	Metal Injection Molding
M _s	Martensite start temperature
NiTi	Nickel-titanium alloy
OM	Optical microscopy
P/M	Powder metallurgy
PVA	Polyvinyl alcohol
RT	Room temperature
SHS	Self-propagating High Temperature Synthesis
SIM	Stress-induced martensite
SMA	Shape memory alloy
SPS	Spark Plasma Sintering
SPT	Space-holder Technique
T	Temperature

1. INTRODUCTION

1.1. State of the Art

1.1.1 Shape Memory Effect & Superelasticity

Since the reveal of superelasticity by Chang and Read in 1951 [1] and shape memory effect by Buehler et.al in 1963, shape memory alloys have been investigated for their superior mechanical properties [2]. Although first industrial occupancy of SMAs was in 1969, further understanding of their shape recovery with phase transformation properties was not achieved until 1980s. The main outstanding property of these alloys is their ability to recover deformation up to 6-7% strain levels whereas metal alloys deprived from strain recovery typically above 0.2% strain level.

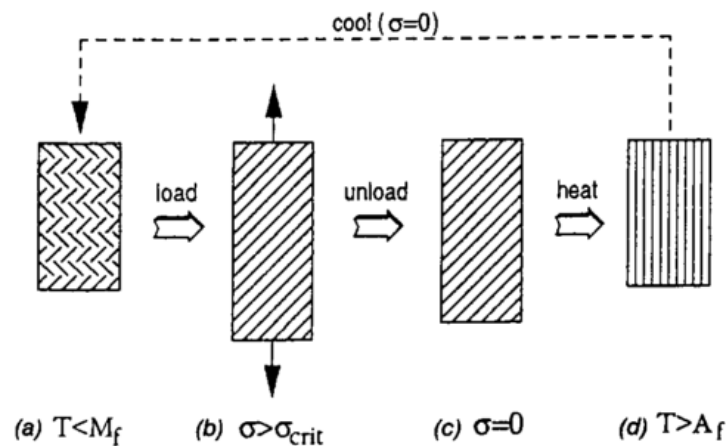


Figure 1 Phase transformation and twinning structure during shape memory behavior [3]

Shape memory effect is the ability of regaining the initial shape after deformation through heating to a specific temperature. This ability is the result of chains of following events which are illustrated in Figure 1 (taken from the study of Brinson, 1993 [3]);

- i. From (d) to (a): twinning of martensite with cooling below austenite start temperature from initial shape.
- ii. From (a) to (b): de-twinning of martensite by loading above a critical stress level.

- iii. From (b) to (c): slight recovery from unloading without any phase transformation.
- iv. Finally from (c) to (d): returning to the initial shape by phase transformation achieved through heating above austenite finish temperature.

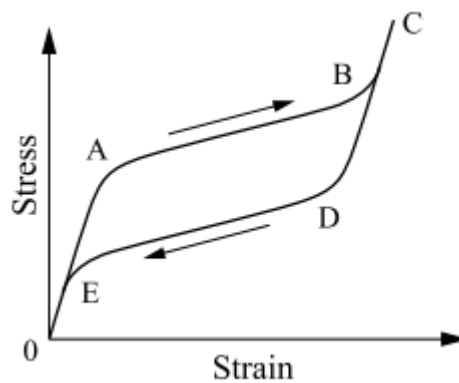


Figure 2 A representative of stress-strain curve of superelastic material [4]

Another unique ability of shape memory alloys is their superelasticity. The superelasticity, which refers to the ability of recovering of high amount of strain (up to 6-7%) after deformation, can be achieved by the martensitic transformation of these alloys by stress without any involvement of heating or cooling processes. Above the austenite finish temperature (where no martensite exists), these alloys can transform into martensitic phase by loading and can restore a certain amount of strain during unloading by reversing this phase into austenite again since the martensite is only formed due to the loading at the first place. This behavior can be achieved until a limit where it is plastically deformed. As a result of this phenomena, a representative curve illustrated in Figure 2 can be observed in an ideal condition. As it can be seen from this figure; the material (in fully austenite phase) exhibits an elastic linear deformation until a certain level of stress ($0 \rightarrow A$); then the stress-induced martensite transformation occurs at a constant (or with a lower elasticity of Modulus, E) stress level ($A \rightarrow B$); after finalization of the diffusionless phase transformation, the material exhibits a similar elastic curve up on further loading ($B \rightarrow C$); then no phase transformation is observed until an

amount unloading (C→D); which is followed by the reverse martensitic transformation results in the higher amount of strain recovery (D→E); and finally the deformed alloy turns back to its original length with an elastic behavior in austenite phase (E→0) [4].

Shape memory behavior is observed in many different metal alloys such as Fe-Pd, Au-Cu, In-Ti, Fe-Mn-Si; however copper-based (Cu-Zn, Cu-Al-Mn, Cu-Al, Cu-Zn-Al etc.) and TiNi-based (Ti-Ni-Cu, Ti-Ni-Hf, Ti-Ni-Pd etc.) alloys are the mainly used materials due to having relatively low costs and other properties such as lower phase transformation temperatures which is one of the main motivations of this thesis [4].

1.1.2 Ni-Ti Shape Memory Alloys

Although the emergence of NiTi alloys among the shape memory alloys are based on biomedical applications due to presenting superelasticity behavior at body temperature, also other superior properties of NiTi, which mainly consist of strength, corrosion resistance, ductility and biocompatibility, made it one of the most commonly used SMAs [5].

Similar to other SMAs, shape memory and superelasticity behavior is dependent on phase transformation temperatures which are mostly affected by its material content, contamination level, deformation and heat treatments. These parameters are examined in detail in below subtopics separately.

a) Material composition

NiTi alloys with 48-52% atomic ratio of Ni content are considered to exhibit shape memory and superelasticity in literature [6]. In Figure 3, the binary equilibrium diagram of NiTi is illustrated. As it can be seen from this figure, solid solution with Ti-rich content is very hard to achieve due to sharp line around 50 atomic % of Ni. However, there is a wider region for slight increase in nickel content for the solid solubility in the alloy. There is also experimental data attached to Figure 3, which is focused on the critical region between 50 to 58% at. Ni in Ti for the temperature range of 627-927°C.

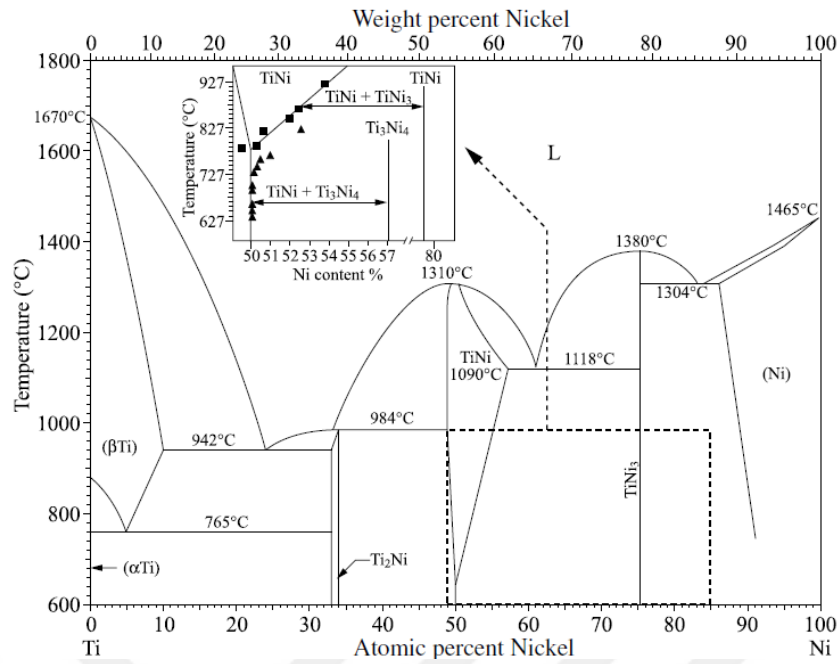


Figure 3 Nickel - Titanium Equilibrium Diagram[4]

In one of his studies, Tang showed the relation between the nickel content and the martensite start temperature in 1997 [7]. The thermoelastic martensite transformation temperature is calculated according to the Gibbs free energy difference between the initial and martensite phases and then compared with experimental results in Figure 4. As it can be seen from the figure, the increase in nickel mole fraction after 50%, results in dramatic decrease in temperature where martensite starts.

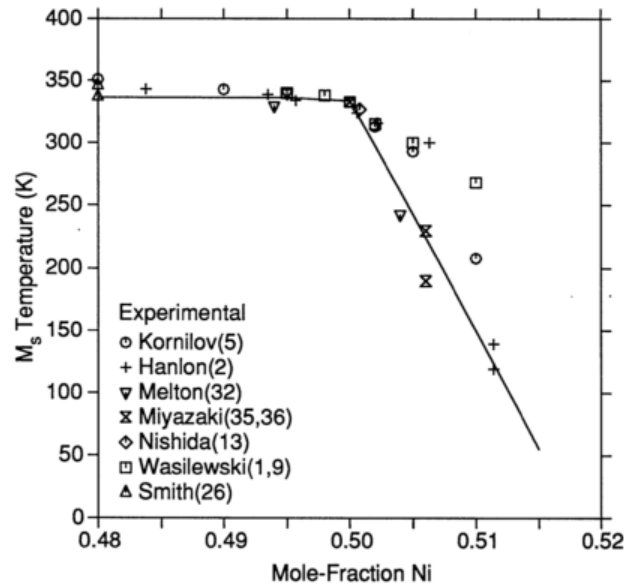


Figure 4 Comparison between theoretical and experimental M_s temperature relation with Ni content in NiTi alloys [7]

b) Contamination

One of the most important issue in both production and characterization of NiTi alloys is the prevention of alloy from chemical contamination. Titanium is a metal which is very reactive to atmospheric elements such as oxygen, nitrogen and hydrogen, especially in high temperature levels. The characteristic of titanium was one of the main reasons which made the determination of binary phase diagram (in Figure 3) until 1980s [8]. In the study of Firstov, the ease oxidation of Ni-50 at.% Ti alloy is analyzed with the temperature dependence and it is observed that the oxidation behavior of NiTi differs in different temperature levels [9]. Until 200°C, there is negligible weight gain of the NiTi specimen according to thermogravimetric measurements. Between 200°C and 500°C interval, oxidation increases linearly, however above 500-600°C temperature, the oxidation amount increases exponentially. Since the more titanium atoms are used in the formation of Ti_4Ni_2O , oxidized NiTi alloys have lower phase transformation temperatures with the higher percentage of Ni staying in the alloy matrix.

c) Heat treatment

Heat treatment, especially aging, is commonly used in NiTi alloys, as it can be seen from the examples from literature in the next chapter. In a specific study of Nishida et.al which was completed in 1986, for observing the intermetallic formation during different aging temperatures and durations, where Ti-50% at. Ni and Ti-52% at. Ni alloy compositions are used [10]. In this study, Ti_2Ni_3 and $Ti_{11}Ni_{14}$ phases are observed with aging processes below $680^{\circ}C$ and Ti_2Ni_3 phase is observed with aging temperature between 680 and $800^{\circ}C$ with the aging duration below 1 hour. Also, it is noted that these undesired formations are increased with the increase aging time. However, at $850^{\circ}C$ aging temperature, no aging products are detected until 9 hours or more aging duration. Since all of the mentioned by-products of aging are rich in Ni content, it can be concluded that aging in NiTi alloys results in increase in austenite start and finish temperatures (as it is mentioned before).

In another study, Aydoğmuş had observed Ni_3Ti_4 formation in a porous NiTi sample, which is produced with space holder technique, after an aging treatment of 1 hour at $400^{\circ}C$, as it can be seen from Figure 5 [8].

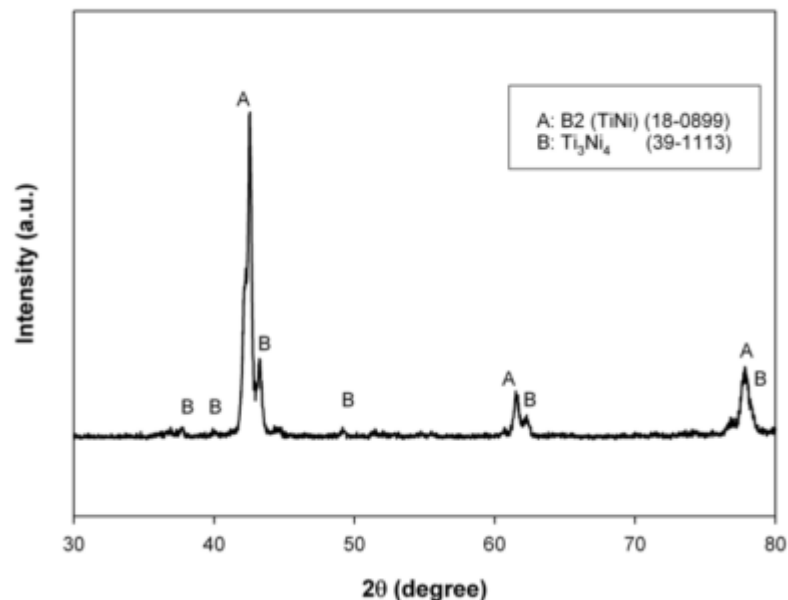


Figure 5 XRD results of NiTi alloy aged 1 hour at $400^{\circ}C$ [8]

As a result, no aging heat treatments were applied in this study, in order to avoid higher phase transformation temperatures and undesired intermetallic formations.

1.1.3 Ni-Ti Alloys with Porosity and Their Characterization in Literature

In the last two decades, porous NiTi alloys have been studied due to two main motivations for increasing the biomedical usage; decreasing the modulus of elasticity compared to bulk NiTi alloy in order to achieve lower values like bones (around 1 GPa) and improving the growth of living tissue through the pores of the material [11].

The porous NiTi alloys, similar to other metal foams, exhibit different properties compared to bulk alloys. Until now, several researches related to production and characterization of porous NiTi alloys have been studied with different manufacturing methods from raw powder materials like hot isostatic pressing (HIP), spark plasma sintering (SPS), self-propagating high temperature synthesis (SHS), metal injection molding (MIM), conventional sintering (CS) and elevated pressure sintering, as some of their examples can be seen from Table 1. In these studies, characterization of porous NiTi alloys with several porosity levels has been done.

Aydogmus, have previously worked on porous NiTi alloys which is produced by two-step conventional sintering methodology with space holder technique and found that also porous NiTi alloys show the superelasticity and shape memory behavior in his PhD. Thesis [8] and several other studies [13]. Addition to this study, Kockar et. al. have investigated the recoverable and irrecoverable strain levels of porous NiTi alloys under increasing constant stress magnitudes produced with the same methodology and concluded that relatively high strength can be observed in Porous NiTi alloys up to 60% porosity with lower densities [12].

Table 1 Some examples on characterization of porous NiTi alloys from literature

Article	Materials used	Production methodology	After treatments	Porosity levels	Loading / unloading tests conducted
Yuan, 2006[13]	Ti – 50.8 at %Ni	a) HIP 3 hours at 1050°C and	0.5 hours aging at	27% porous (HIP),	4% strain at room T (26°C)

		150 MPa b) CS 3 hours at 1050°C	450°C, Quenched	43% porous (CS)	
Zhang, 2007 [14]	Ti – 50.8 at %Ni	HIP 3 hours at 1050°C and 150 MPa	0.5 hours aging at 450°C, Quenched	Dense, 27% porous,	Cyclically loaded at 1% to 8% strain No temperature info
Bassani, 2009 [15]	equiatomic NiTi	SHS , no specific information	None specified	30 – 68 % porous	6% strain at room temperature and 110°C (above A _r)
Zhao, 2005 [16]	Ni – 50.9 at.%Ti	SPS , 5 min.	0.5 hours heat treatment at 320°C, Quenched	Dense, 13% porous, 25% porous	Compression tests with 4.5%, 5.3% strain
Guoxin, 2008 [17]	equiatomic NiTi	MIM : Injection at 40 MPa, 80°C feedstock and 55°C mold temperature, Debinding solvent at 5-55°C Vaporizing at 400°C	None	75% porous	None
Li, 2009 [18]	Ti – 50.8 at %Ni, TiH _{1.5} as space holder	a) SPT with titanium hydride, LPS 3 hours at 5 MPa and 1050°C b) CS , 3 hours at 1050°C	0.5 hours aging at 450°C, Quenched	15% porous, 30% porous, 33% porous, 46% porous	4% strain compression tests at 50 °C (above A _r)
Aydogmus, 2012 [19]	Ti – 50.6 at %Ni, 450 µm Mg powders	SPT with magnesium, 1 hour CS at 1100°C	aging at 450°C	38% porous, 51% porous, 59% porous	Different compression tests up to 250 MPa at room, body and above A _r temperatures
Bandsiddhi, Dunand, 2008 [20]	48.6 at. %Ni, NaCl	SPT with NaCl, 4 hours HIP at 950 or 1065°C, 2 days for dissolution of NaCl, 4hours or 24 hours additional sintering at 1250°C	5 min oil bath at temperature above A _r , Oil- quenched, 20 min cleaning in acetone	32-36% porous	Loading and unloading up to 8% strain at room and body temperatures
Li[21]	49.2 at. %Ti Urea	1 hour sintering for removal of urea (SPT) 3 hours CS at 1000/1100°C	0.5 hours aging at 450°C, Quenched	31-47% porous	Compression test at 2.5 and 3% strain levels at room temperature
Zhang, 2007 [22]	Ti-51 at. %Ni, Ammonium bicarbonate (NH ₄ HCO ₃)	Decomposing 30 min at 200°C (SPT) 3 hours CF-HIP at 1050°C and 50 MPa	2 hours aging at 450°C, Quenched	30-48% porous	None

In this study, porous NiTi samples were produced by conventional sintering with space holder technique such that this method has been applied and validated by other researchers in the last decade.

1.2. Objective

The main objective of this thesis is to produce innovative high energy output materials with enough strength but lower density by determination of stress vs temperature phase diagrams and superelasticity characterization of NiTi alloys with 10%, 20%, 30% and 40% porosity levels was conducted to find out the superelastic temperature window in which the porous samples can be used as dampers or actuators.

Although there are studies about the phase diagrams of Ni-rich bulk NiTi alloys, the thermomechanical characterization of porous Ni-rich NiTi alloys will be the original contribution in this thesis. By obtaining the stress vs temperature phase diagram and M_d temperatures of porous NiTi alloys with different porosities, the thermomechanical properties will be obtained and therefore, the new usage areas other than medical biomaterials such as aerospace applications can be identified.

1.3. Expected Impact

The porous NiTi alloys are promising for many engineering applications, especially aerospace engineering, due to having low densities with similar mechanical properties compared to other conventional materials. These advantages of porous NiTi alloys can provide lower weight applications with almost the same strength with lower energy consumption in aero-engineering and in many other fields. Actuator type of applications (doing work against the applied load) is very important since replacing heavy motors with these novel and smart materials will be the main aim to lower the weight of the structure and minimize the energy consumption together with reducing the fuel consumption.

The added value of this thesis will be determining the stress vs temperature phase diagram and M_d temperature of the foam SMAs with different porosity levels, which

will designate not only thermomechanical characteristics but also the working temperature interval of this promising alloys for new or existing application fields.

The overall expected impacts within the light of this study are;

- To replace heavy motors by lowering the weight (as an actuator working against the applied load in aerospace applications) and minimizing the energy consumption with decreasing fuel consumption,
- To fulfil the lack of information about the stress vs temperature phase diagrams and the superelastic temperature range of porous NiTi alloys in the literature.



2. LITERATURE REVIEW

2.1. Production of Porous NiTi Alloys

2.1.1 Existing Porous NiTi Production Methodologies

There are different metal foam production techniques in the state of art which mainly consist of liquid state processing, vapor deposition, electro-deposition method and solid state processing (Powder Metallurgy). However, all of these techniques except powder metallurgy (P/M) are not commonly used for obtaining porous NiTi alloys in literature [8]. Powder metallurgy methodologies provide control over the porosity levels by adjusting the powder amounts and working at lower temperature (below melting point unlike liquid state processing) with relatively lower energy and investment costs (unlike laser sintering with expensive equipment requirements). Moreover, atmospheric reactivity of NiTi alloys prevents the techniques which have the involvement of gas injection or forming like in some liquid state processing methodologies [23]. Intolerance of chemical contamination in NiTi alloys also eliminates techniques which contain polymeric materials used as mold or foam formation agent.

2.1.2 Powder Metallurgy Techniques used for Porosity Formation

In this subchapter, existing powder metallurgy methodologies which are used in previous production of porous NiTi are summarized.

a) Self-propagating High Temperature Synthesis (SHS)

As one of the most used production methodologies, SHS uses self-propagation of preheated powder compacts with starting an ignition from one end [24, 25, 15, 26, 27, 28, 29]. The steps of this fast (around 5 minutes for TiNi production) methodology are shown in Figure 6 [25].

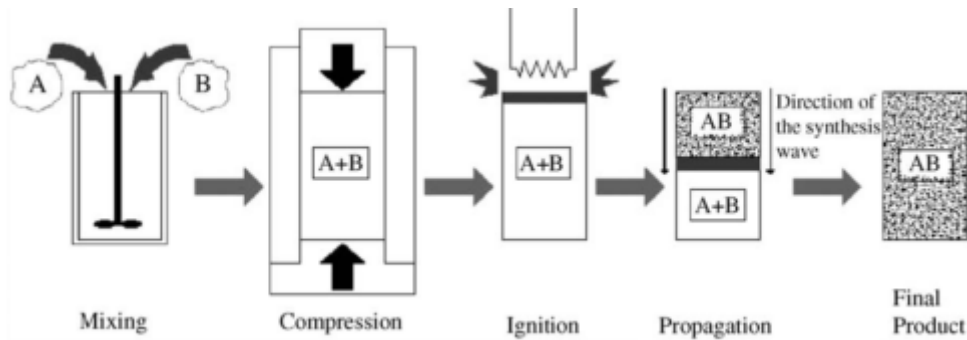


Figure 6 Illustration of SHS methodology [25]

The preheating is only necessary for some of the materials which have low exothermic reaction energies for the synthesis such as the reaction between Ni and Ti [8]. However, this uncontrolled reaction chain may result in other intermetallic synthesis such as Ni_4Ti_3 , Ti_2Ni and Ni_3Ti which are detected in previous studies with XRD analysis [24, 26]. Formation of these undesired compounds either requires additional after treatments or causes poor shape memory and super-elasticity behavior. Additionally, the pore distribution and porosity levels achieved with SHS, are hard to control. These disadvantages of SHS methodology are also given in Table 2, at the end of this subchapter.

b) Hot Isostatic Pressing (HIP)

Another type of powder metallurgy technique, hot isostatic pressing is also commonly used in the production of porous NiTi [13, 30, 31, 32].

As it can be seen from Figure 7, the intended powders are cold-pressed with the permission to trap gas between powders. Then the loosely compacted powder heated to $950\text{-}1050^\circ\text{C}$ (below melting temperatures) and pressed to $100\text{-}200\text{ MPa}$. This process provides trapped gas to expand and form pores in the specimen. NiTi specimens produced with HIP shows relatively good thermomechanical properties, however the oxidization of specimens is not avoidable during the gas trapping process and the pore sizes are relatively low. In order to increase the porosity levels and the pore sizes, space holder technique with agents of sodium chloride and ammonium bicarbonate is combined with HIP methodology in some studies

[20, 22]. The results obtained with these space holder agents are summarized in the next subchapter of this study.

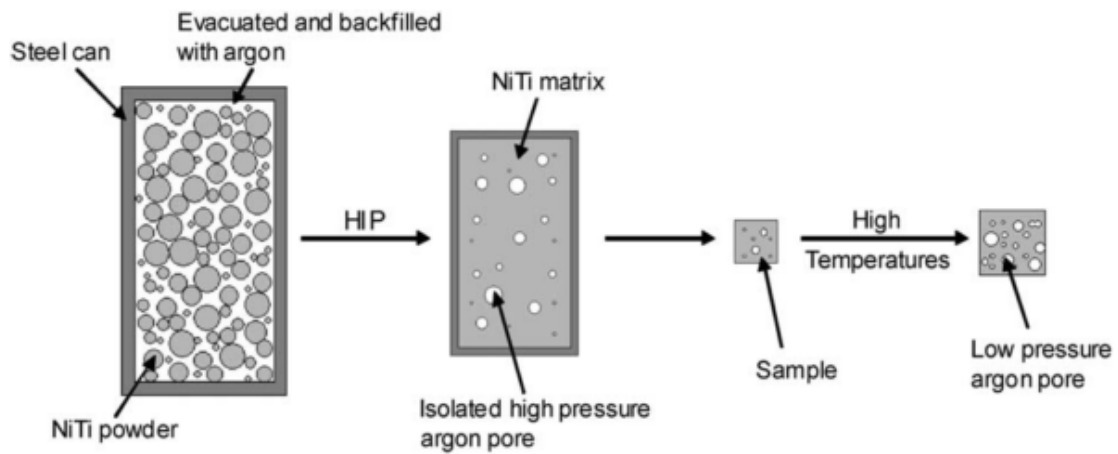


Figure 7 Illustration of HIP methodology [30]

c) Spark Plasma Sintering (SPS)

The first application of SPS for the production of porous NiTi has been completed under the study of Zhao et.al [16]. The pulsed or un-pulsed current is fed to a graphite die which contains the compressed powder mix, and the internal excessive heat generation within the specimen provides sintering in low temperatures and very short time around 5 minutes. Another advantage of this methodology is the ability of the surface purification during spark discharge, which cleans the surface of the specimen. Although this methodology has advantages like short sintering time (low oxidization potential), low working temperatures and good super-elasticity behavior; the pore size and pore distribution among the porous NiTi specimens are found to be inhomogeneous and uncontrolled.

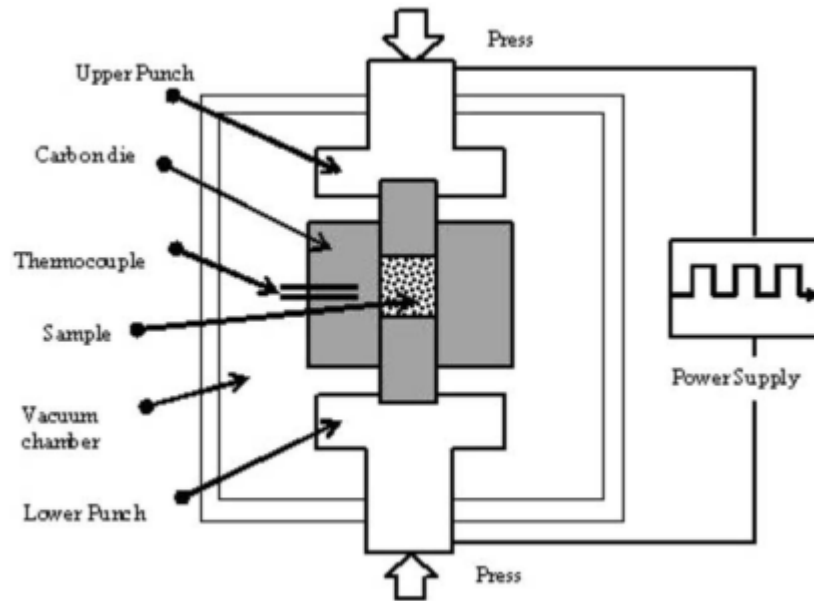


Figure 8 Illustration of SPS methodology [16]

d) Metal Injection Molding (MIM)

In the study of Guoxin et.al metal injection molding, which can be described as the combination of SHS and plastic injection molding techniques, is used for the production of porous NiTi samples [17]. This procedure includes the feeding of bonded metal powders into a mold with an injection pressure of 400 bar and temperature at 80°; Debinding of polymers; and self-propagating combustion. Cleaning of the binder was not achieved fully and the intermetallic formations are observed due to SHS [17].

Table 2 shows the main problems faced during these discussed production methodologies. Some of the problems like oxidization and contamination could not be avoidable in all methodologies, however mitigation suggestions like magnesium space holder agent will be discussed in this study.

Table 2 Comparison of porous NiTi production methodologies and common problems

Production method	Problems	Results in
Powder metallurgy [19]	Undesired intermetallic compounds	Brittleness, poor superelasticity

CS	Long sintering process	Increased time to exposure to ambient and hence oxidation
SHS[18]	High porosity levels, large pore sizes	Poor mechanical properties and superelasticity
SHS[17]	Formation of intermetallic compounds	Poor mechanical properties and superelasticity
CS, SHS, HIP [16]	Brittle samples	Lower ductility
CS, SHS, HIP [16]	Long production phase	Undesired reaction products
HIP and CF-HIP	High pressure and high temperature	Increased production costs
CS, HIP, SPS [19] SHS, SPS [20]	Uncontrolled pore size and shape	Poor mechanical properties Poor biocompatibility (less than 100µm)
SHS, CS, SPS [19]	Irregular pore size and pore distribution	Higher stress (singularity?)
All (specifically MIM and SHT) [19]	Contamination	Poor mechanical properties
All [19]	Sensible and reactive to atmospheric elements (O, C, N, H)	Poor mechanical properties

2.1.3 Space Holder Technique and Magnesium

In previous studies, different agents used as space holder in the production of porous NiTi samples, such as ammonium bicarbonate (NH₄HCO₃), urea and NaCl as it can be seen from Table 1 [20, 21, 22]. In all of these methodologies, several problems have been faced during the cleaning process of these discussed agents. The agents are needed to be melted with heating procedure or dissolved in water in order to be removed from the specimens. These procedures mostly contaminate NiTi specimens directly (without being cleaned fully from the specimen) or indirectly (due to reactivity of NiTi to atmospheric and other elements which are discussed in previous section).

Magnesium is firstly used by Esen and Bor for the production of porous NiTi alloy in 2007 and other studies which involve magnesium as space holder followed [33, 11, 12]. The main advantages of magnesium can be listed as follows:

- The solubility of magnesium in nickel or titanium is very low. This prevents the other intermetallic formation.
- The affinity of magnesium to oxygen and some other elements is higher which prevents the oxidization of samples (Table 3).

- Magnesium can be fully boiled at 1090°C which is below the sintering temperature. There is no requirement of additional procedure for the removing of space holder.
- Magnesium is a biocompatible material like NiTi. Mg is not damaging this characteristic of NiTi in case of any remnants.

Table 3 Formation energy of magnesium, nickel and titanium compounds in the working temperatures [8]

Compound	Formation energy, ΔG_f (kJ/mol)		
	1100 ° C	1200 ° C	25 ° C
MgCO ₃ (Magnesium Carbonate)	-	-	-1012.186
MgH ₂ (Magnesium Hydride)	-	-	-36.713
Mg ₃ N ₂ (Trimagnesium Dinitride)	- 157.537	- 107.370	- 400.498
Mg(NO ₃) ₂ (Magnesium Nitrate)	-	-	- 589.182
MgNi ₂ (Magnesium 2-Nickel)	-	-	- 54.119
MgO (Magnesium Oxide)	- 442.919	- 422.096	- 568.943
MgOH (Magnesium Monohydroxide)	- 182.711	- 173.499	- 172.480
Mg(OH) ₂ (Magnesium Hydroxide)	-	-	- 833.644
NiCO ₃ (Nickel Carbonate)	-	-	- 617.876
Ni(CO) ₄ (Nickel Tetracarbonyl)	- 545.260	- 541.551	- 587.249
NiO (Nickel Oxide)	- 115.193	- 106.753	- 211.539
NiTiO ₃ (Nickel Titanium Trioxide)	- 816.664	- 789.789	- 1118.188
TiNi (Titanium Nickel)	- 52.636	- 51.019	- 65.546
Ti ₂ Ni (2-Titanium Nickel)	-	-	- 78.034
TiNi ₃ (Titanium 3-Nickel))	- 106.497	- 103.215	- 134.204
TiC (Titanium Monocarbide)	- 167.788	- 166.292	- 180.844
TiN (Titanium Mononitride)	- 205.779	- 196.429	- 309.155
TiO (Titanium Monoxide)	- 409.957	- 401.244	- 513.278
TiO ₂ (Titanium Dioxide, Rutile)	- 691.634	- 673.947	- 889.406
Ti ₂ O ₃ (Dititanium Trioxide)	- 1138.082	- 1112.637	- 1433.824
Ti ₃ O ₅ (Trititanium Pentoxide)	- 1843.391	- 1801.840	- 2317.294
Ti ₄ O ₇ (Tetratitanium Heptaoxide)	- 2539.272	- 2479.914	- 3213.016
TiH ₂ (Titanium Dihydride)	50.036	64.148	- 105.073

2.2. Superelasticity Characterization

2.2.1 Maximum Temperature to Induce Martensite (M_d)

Shape memory and superelasticity behavior is observed in shape memory alloys depending on the temperature levels, since these behaviors are related to martensite and austenite phase transformations. As it can be seen from Figure 9, below austenite start temperature, one can observe shape memory effect. On the other hand, above austenite start temperature, superelasticity can be achieved

[34]. This figure also demonstrates two different type of deformation behaviors of shape memory alloys as two different curves;

1. The critical stress for slip decreases with increasing temperature, since it is easier to deform materials at higher temperatures similar to conventional metals.
2. The critical stress to induce martensite with loading increases with increasing temperature, because austenite phase is more stable at higher temperature and higher stress levels are required to induce martensitic transformation at higher temperature [34].

The main objectives of this thesis are to observe superelasticity behaviour and to determine M_d temperature (maximum temperature to induce martensite with loading). As a schematic stress-temperature diagram, Figure 9 illustrates two main criteria for observing superelasticity as following:

1. Critical stress for slip should be lower that critical stress to induce martensite,
2. The temperature should be higher than austenite start temperature (A_s).

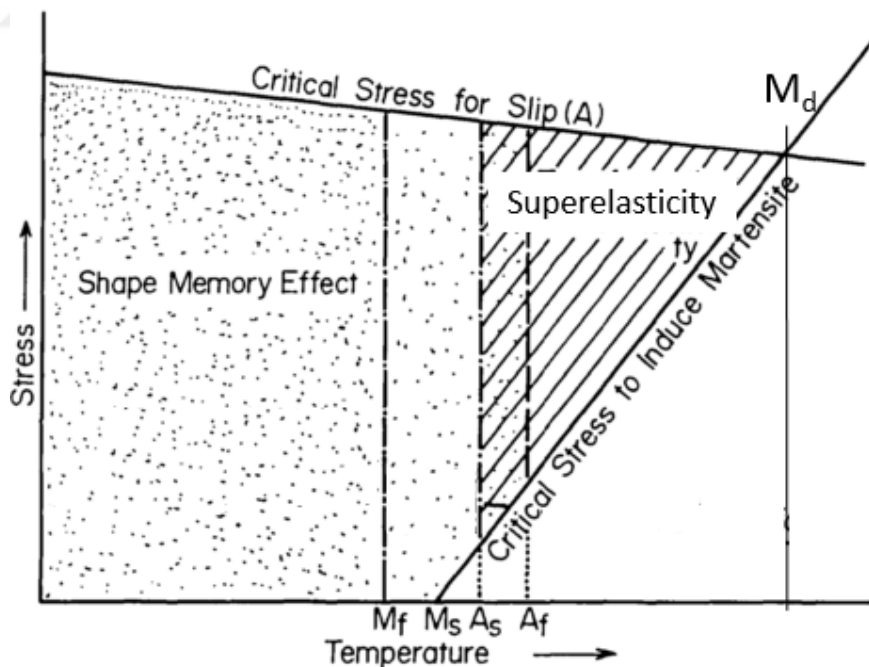


Figure 9 Representative Stress vs Temperature Phase Diagram of Shape Memory Alloys [34]

To sum up, M_d is the highest temperature level where the critical stress for slip curve and critical stress to induce martensite curve meet. Hence, by determining M_d temperatures for porous NiTi alloys lower one can know the superelastic temperature window of this type of shape memory alloys.

2.2.2 Superelasticity Behavior of Porous NiTi Alloys Produced with SPT

Although there are no studies conducted earlier for the determination of M_d temperature of porous NiTi alloys, the superelasticity behavior of Ni-rich porous NiTi alloys is found promising for several applications in literature as discussed earlier.

In Figure 10, superelasticity behavior of 37% (a) and 43% (b) porous Ni-rich NiTi samples are shown from a previous study where space holder technique with magnesium is firstly used [8]. In this figure, different compression tests conducted on room temperature for 37% porous (which is sintered one hour at 1100°C) and 43% porous specimen (which is sintered two hours at 1200°C like this study) are illustrated. In both of the porosity levels, aged specimens showed lower strength and worse strain recovery than as-processed ones at same deformation amounts. Obtaining worse strain recovery from aged specimens is also related with higher phase transformation temperatures (and therefore higher critical stress levels to induce martensite) resulted in aged specimens. These are some of the reasons why no aging treatment is applied in this thesis. However, full strain recovery was not observed in porous NiTi specimens at room temperature as well as at temperatures higher than austenite finish temperature, although it was observed in bulk samples produced with the same sintering processes [8].

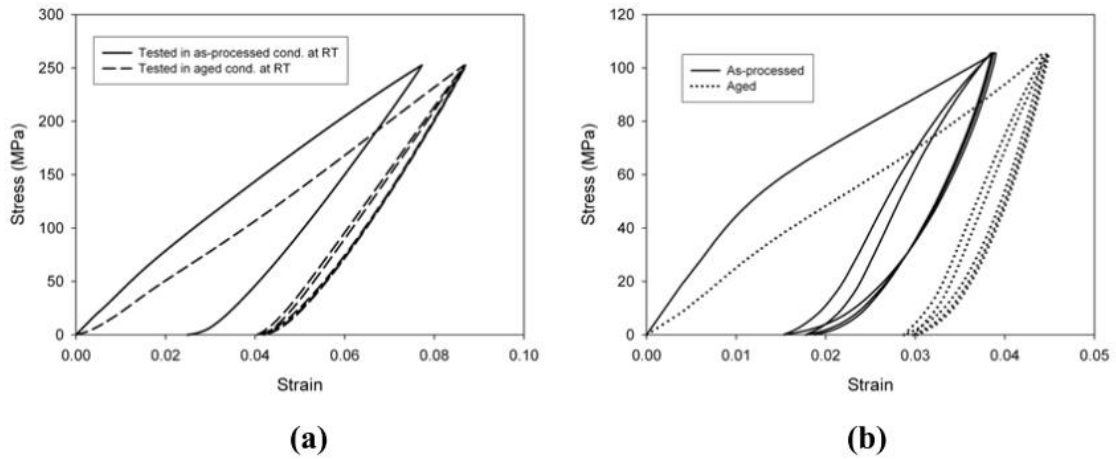


Figure 10 Compression test results (RT) of 37% and 43% porous NiTi specimens with different production and aging processes from literature [8]

In Figure 11, higher strain levels are tested for the same specimens at temperature above A_f . Higher stress levels and higher strain recovery amounts were observed in compression tests completed at this temperature level than room temperature, as expected.

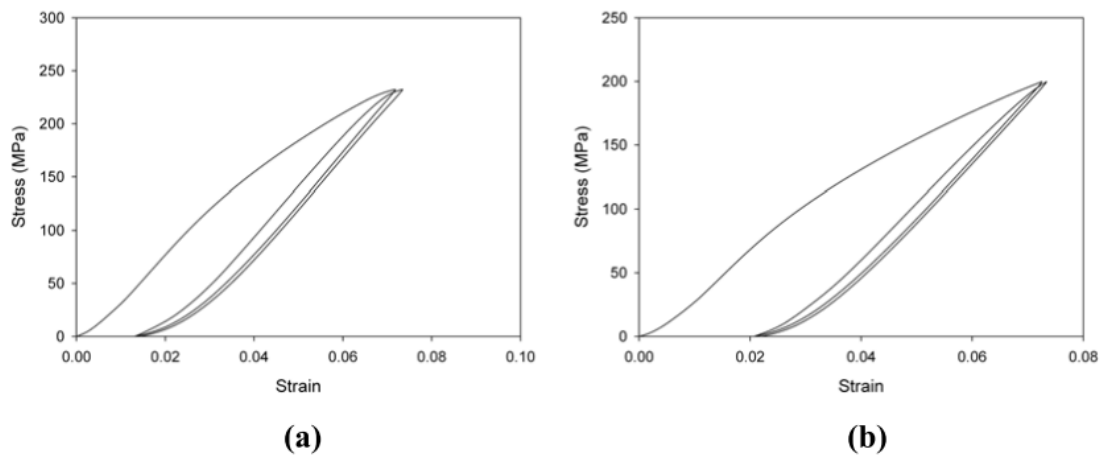


Figure 11 Compression test results (above A_f) of 37% and 43% porous NiTi specimens with different production and aging processes from literature [8]

3. EXPERIMENTAL PROCEDURE

The experimental procedure of this thesis basically consists of two phases; production and characterization (thermal, microstructural and thermomechanical).

The production phase of porous NiTi alloy specimens consists of powder mixing, pressing and sintering. The magnesium and NiTi pre-alloyed powders are mixed in the amount of the desired percentages (according to desired porosity levels) and then pressed with a hydraulic press machine. These pressed but weak specimens (having a certain green density), are put in vertical and atmosphere controlled sintering furnace in order to remove the magnesium powders by evaporation (void formation) and to sinter and strengthen these specimens. Magnesium powders evaporate and leave their positions to pores in the first phase of Conventional Sintering (CS) through which the samples are heated from room temperature to 1100°C with the heating rate of 10°C/min and stay an hour at 1100°C. Then the samples are further heated to 1200°C to obtain full sintering and high strength foam materials. In this study, specimens with 0, 10, 20, 30 and 50 percent of porosity levels are aimed. Magnesium powder size range is chosen as 250µm-600µm since the human tissue size is in the same range such that the human tissue growth can become possible through the pores. It is worth mentioning that no heat treatment (aging etc.) is conducted after sintering of the specimens, because it is proven that aging results in higher phase transformation temperatures and superelasticity behavior of porous NiTi alloys were demonstrated in previous works [35, 36, 12].

After the production of NiTi specimens, the porosity levels and pore shapes of specimens are measured and observed via using optical microscopy (OM). Furthermore, the microstructural analysis were also conducted to determine the intermetallic phases in the samples. The transformation temperatures of specimens are determined by Differential Scanning Calorimetry (DSC) technique in order to obtain the temperature intervals (M_s , M_f , A_s and A_f) of martensitic and austenitic transformations of the samples having different porosity levels. In addition, the thermal hysteresis magnitudes of specimens are calculated by taking the difference between the martensite peak and austenite peak temperatures in DSC curves. The final procedure for the determination of the stress vs temperature phase diagram of porous NiTi specimens is the conduction of

superelasticity experiments by loading until to 3% with constant strain rate and unloading with constant force rate, while increasing the temperature by 30°C after every loading-unloading cycles starting from $M_s+15^\circ\text{C}$ in compression test set-up. The stress levels to induce martensite at different temperatures are found and also the strength of the samples via loading the samples to 3% strain level in the austenitic phase is determined. Stress vs temperature phase diagrams of the samples will be generated and the maximum temperature at which the martensitic phase transformation in each samples is achieved (M_d) is determined.

3.1. Production of Specimens

3.1.1 Materials Used

Ni-49.6 at. %Ti powder (50.4 to 49.6 atomic ratio of Ni to Ti), which has average particle size of 17.6 μm together with pure magnesium powder with changing diameter between 250 to 600 μm are used in the production. In order to keep the green samples together before sintering, polyvinyl alcohol solution is added in each specimen with the amount of 5% of its total powder mass. PVA solution is obtained by solving the PVA powder within distilled water in different amounts of weight percentages between 2.5 to 3.6 with the help of heating and stirring device, in order to achieve an optimum binding of NiTi and Mg powders.

The estimated material amounts used for the preparation of the specimens according to porosity levels can be found in Table 4. These amounts are calculated for having different volumetric percentage of Mg in compressed NiTi powder, in accordance with their densities.

Table 4 Estimated material amounts for porous NiTi

Porosity Levels	Volume (cm^3)		Mass (g)		
	Mg	Niti	Mg	Niti	PVA
0%	-	0.942	-	6.136	0.307
10%	0.094	0.848	0.164	5.522	0.284
20%	0.188	0.754	0.328	4.908	0.262
30%	0.283	0.660	0.492	4.295	0.239
40%	0.377	0.565	0.656	3.681	0.217
50%	0.471	0.471	0.820	3.068	0.194

The mixing of powders is one of the important phases of production, since achieving homogenous pore distribution is highly dependent on mixing duration. In this thesis, powders and PVA are mixed manually around 15 – 40 minutes until the magnesium particles are all covered with NiTi powder. Although 30 minutes of mixing is suggested as an optimum time period for homogenous distribution in the study of Aydoğmuş, since, some powder mixtures of Mg and NiTi were separated from each other after 15 minutes of mixing [8]. Therefore, the mixing duration was determined by experience rather than solid time duration in this study.

3.1.2 Hydraulic Pressing

All of the powder mixtures are compressed with the help of a uniaxial hydraulic pressing machine and steel mold having 10 mm diameter which can be seen in Figure 12. A mold release agent was applied to the mold before pouring down the powder mixtures. A pressure range between 190 to 1150 MPa had been tested in order to obtain the optimum level and 400 MPa was found the most efficient stress magnitude in an earlier study [8], since 400 MPa is enough to achieve a good compact and low enough in order not to deform Magnesium powders. Therefore, same pressure level was applied in this study and cracks or non-uniformed distribution of particles were not observed due to compression process of specimens.



Figure 12 Three parts of P/M mould and hydraulic pressing machine

3.1.3 Two-step Conventional Sintering

Before the conventional sintering process, all specimens were prepared as following (see Figure 13):

- Green specimens were located into a crucible made of MgO with additional magnesium particles for preventing oxidation.
- The MgO crucible and the specimen were put into the specimen holder which is made of Ti6Al4V. The MgO was located between the specimens and Ti6Al4V holder in order to prevent the possible reaction in between NiTi and Ti6Al4V.
- The separator was placed for creating another zone before specimen with Ti sponges in order to block oxygen reaching to the specimen.
- The main cover then was placed on top of the holder (see Figure 14).

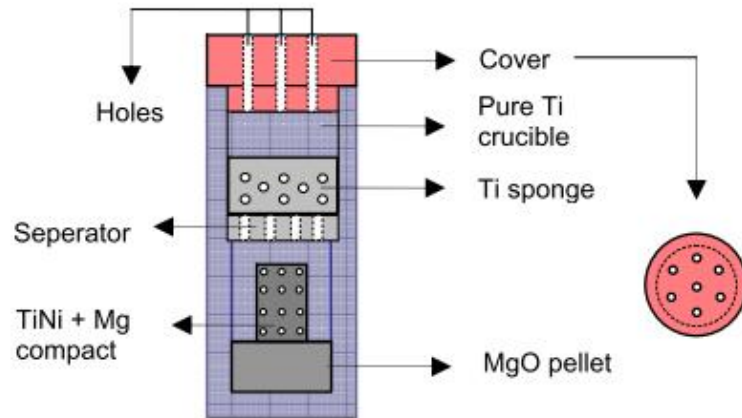


Figure 13 Illustration of specimen holder set-up used during conventional sintering [8]



Figure 14 Ti6Al4V specimen holder

After the preparation of the specimen with the holder, two-step conventional sintering was applied to all green compacted specimens in the sintering furnace which is isolated from atmosphere for obtaining pure argon environment as shown in Figure 15. The steps of the sintering process are listed below:

- Increase temperature to 1100°C from room temperature by 10°C/min
- Hold temperature at 1100°C for 1 hour
- Increase temperature to 1200°C from 1100°C by 10°C/min

- Hold temperature at 1200°C for 2 hours

The temperature control was done according to the thermocouples placed in the middle of the ceramic tube where the specimen was hung with the aid of a steel wire rope. There were no other thermocouples in the sintering set-up, therefore the temperature of the cooling zone was unknown. The cooling zone which was at the top of the vertical furnace was cooled down constantly with the use of water flowing through copper tubing as it is shown in Figure 15.



Figure 15 Conventional sintering furnace and high purity argon-filled tube

After the sintering was ended, the specimens were pulled up to the cooling zone of the furnace without exposing them to the atmosphere. The cooling was relatively slow however this was necessary for prevention of the oxidation. As mentioned before, the cooling was maintained with copper tubes wrapped around the ceramic tube of furnace and circulation of tap water through this tubing. The 99.999% pure argon supply to the furnace was kept during both the sintering and cooling phases for avoiding the oxidization of specimens since NiTi alloys have very high potentials to oxidation above 200°C.

3.2. Macro-porosity Calculations

In order to determine the real porosity amounts of the sintered specimens, the images of the macrospores having sizes 50-600 micron were taken by a camera which is attached to the optical microscope and a digital image analyzing program was used to determine the porosity percentage of the produced samples.

Firstly, the surface of the specimens were grinded and polished for obtaining scratch-free and smooth surfaces after the cutting procedure, by the aid of Metkon Forcipol Grinder & Polisher machine (Figure 16). The specimens which were produced with 10%, 20%, 30%, 40% (in volume) and no magnesium additions, were grinded with sandpapers which have 320, 400, 600, 800, 1000, 1200 and 2000 microns abrasive particles, respectively. After the grinding, all of them were polished with diamond suspensions of 6, 1 and 0.25 microns.



Figure 16 Grinder and polisher

The macro porosity levels of specimens were calculated with Nikon optical microscope and Clemex Image Analysis Software. The used optical microscope was equipped with 50x, 200x, 500x and 1000x magnification lenses. Different images were captured from the surfaces of the specimens, which were grinded and polished beforehand, with different magnification levels.



Figure 17 Optical Microscope and the attached Camera

After the collection of the images from surface, these images were filtrated according to their grey area and the area percentage of the pores were calculated with this software. An example from one of the images collected for 10% porous specimen is illustrated in Figure 18. As it can be seen from this figure, the macro-porosities of the specimens are calculated according to the average grey size areas collected from different areas over the surfaces.

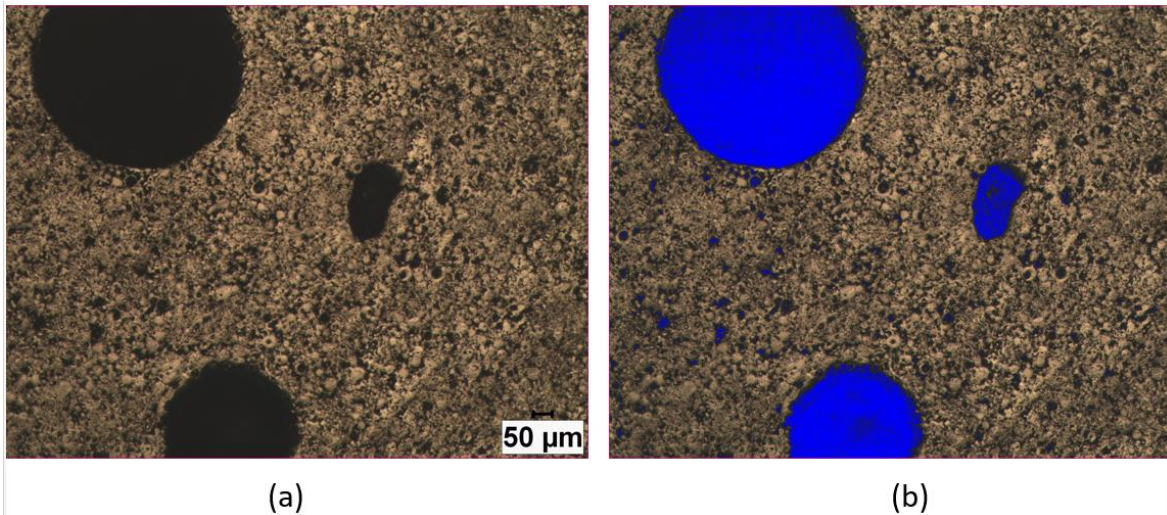


Figure 18 Example of the macro-porosity imaging of 10% porous specimen with Clemex Image Analysis software (a) image from the surface, (b) grey area scope used in image analysis calculations

3.3. Metallographic Imaging

For the observation of martensite and austenite phases (depending on the phase transformation temperatures of the specimens) at room temperature, additional etching had been applied to the specimens after grinding and polishing procedures.

Two different etching solutions were used for the specimens which are martensite and austenite in room temperature. For the specimens with martensite phase (10% porous and 20% porous specimens), HF + HNO₃ + CH₃COOH mixture is applied with 1:4:5 ratio scale, respectively [37]. On the other hand, a mixture with equal amount of HCl, HNO₃ and acetic acid, which attacks grain boundaries particularly, is used for the specimens with austenite phase (bulk, 30% porous and 40% porous specimens) [38]. The exposure time to acid mixtures are determined step-by-step with 10 or 20 seconds intervals by controlling the images with optical microscope at every step in order to avoid overexposure on the surface of specimens.

3.4. Differential Scanning Calorimeter Analysis

Differential Scanning Calorimeter (DSC) was used for the thermal characterization of dense and porous specimens. It is very important to determine the

transformation temperatures of the produced samples for deciding the temperatures at which the superelasticity experiments are conducted.

3.4.1 Specimen Preparation

The specimens were cut for obtaining an appropriate dimensions and weight for DSC analysis with a diamond coated disk by Micracut 150 precision cutter machine (shown in Figure 19). During the cutting phase of the specimens, cutting speed was kept at minimum levels without exceeding 100 rpm, because higher cutting speeds induce stresses to samples and this alters the phase transformation temperatures [36].



Figure 19 Precision cutter used

3.4.2 DSC Analysis Procedure

DSC analyses of all specimens were completed through Perkin Elmer DSC 8000 equipment by heating and cooling them between -80 or -70 and 150°C with heating-cooling rate of 10°C/min. The heating and cooling cycles were repeated three times and the last cycle was used for determination of phase transformation temperature which is more reliable than that of the first two cycles as suggested in ASTM F2004-05 standard.

Here is the DSC experiment procedure which was applied to all of the specimens:

1. Hold for 1.0 min at 30.00°C
2. Cool from 30.00°C to -70.00°C at 10.00°C/min
3. Hold for 1.0 min at -70.00°C
4. Heat from -70.00°C to 150.00°C at 10.00°C/min
5. Hold for 1.0 min at 150.00°C
6. Cool from 150.00°C to -70.00°C at 10.00°C/min
7. Hold for 1.0 min at -70.00°C
8. Heat from -70.00°C to 150.00°C at 10.00°C/min
9. Hold for 1.0 min at 150.00°C
10. Cool from 150.00°C to -70.00°C at 10.00°C/min
11. Hold for 1.0 min at -70.00°C
12. Heat from -70.00°C to 150.00°C at 10.00°C/min
13. Hold for 1.0 min at 150.00°C
14. Cool from 150.00°C to -70.00°C at 10.00°C/min

3.5. Superelasticity Tests

The uniaxial compression tests are conducted with Utest material test equipment with servo-mechanical test frame, which has 50 kN capacity. All specimens are loaded up to 3% strain magnitude with a constant strain rate of 0.1 mm/min. Unloading phase is limited with force control in order to observe any unrecovered strain amounts.

Higher load magnitudes should be applied to shape memory alloys to get the stress induced martensite with the increase in temperature during loading, therefore all loading and unloading tests are generally performed starting with 10 or 20°C higher than austenite finish temperatures of the samples in order to observe superelastic behavior [19]. In our study, all loading tests are performed starting above $M_s + 15^\circ\text{C}$ and the test temperature is increase in each loading cycle to obtain the M_d temperature. The heating coils (made of copper) are attached to the crossheads which are in contact with the tested sample therefore the heating is maintained by conduction. Temperature control is done using the data measured by the thermocouples located just under the contact surface of

samples for obtaining the closest temperature value. All tests are completed under constant temperature; however between each cycles, a heating rate of 10°C/min is used. The heating coils and the space between the crossheads are covered with insulation material in order to reduce the heat loss to the environment.

In this study, all of the mechanical analyses are conducted with the data obtained from a high temperature extensometer which is attached to the marked locations on crossheads which are approximately 1.5 mm above and below the specimen gap. The extensometer is connected to the crossheads with ceramic rods. The gauge length of the extensometer is altered with respect to the length of specimens (changing 10.1 to 11.6 mm); however it is worth noting that all lengths were in the working interval of the extensometer. In order to achieve accurate data collection, the extensometer is connected parallel to the ground.

The compression test set-up explained above and the programming user interface can be seen in Figure 20 and Figure 21.



Figure 20 Superelasticity test setup with extensometer

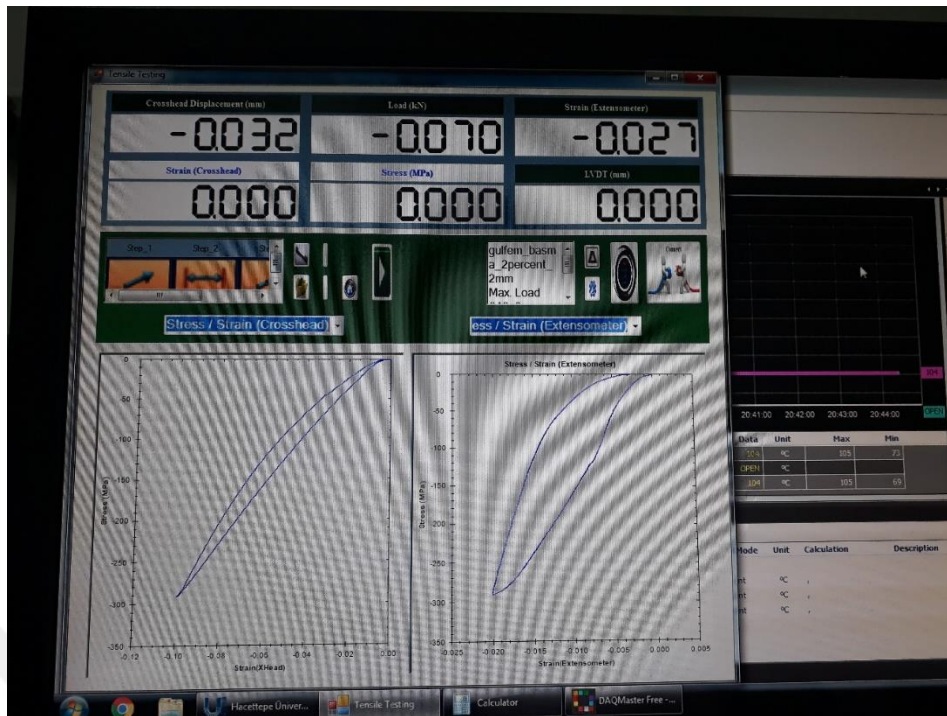


Figure 21 Compression test graphical user interface during a conducted test

4. RESULTS & DISCUSSION

4.1. Production Process Review

The material amounts used during the production are listed in Table 5. One can see from Table 5 that porous specimens have lost their mass approximately in the amount magnesium powder added which is an expected pattern and this proves that magnesium content is safely removed from the alloy. However, the changing mass in dense specimen can be explained as the loss during the holding and preserving time period of green NiTi samples, as well as the loss of PVA which is not volatilized during the storing. As it can be seen from this table that a couple of mass values of the specimens are missing after sintering because their masses could not be compared with previous masses in a meaningful way due to the extreme oxidization. Further discussions related to oxidization can be found in the following chapters of this thesis.

Table 5 Amounts of material used in specimens

Specimens		Materials used			Mass of green sample (A) g	Mass of sintered specimen (B) g	(A-B) g
		Mg powder	NiTi powder	PVA solution			
		g	g	g			
Dense	1st	-	6.647	0.332	6.564	6.502	0.062
	2nd	-	6.142	0.318	6.077	N/A	N/A
	3rd	-	6.137	0.310	6.031	5.998	0.033
10% porous	1st	0.341	11.470	0.750	11.376	10.885	0.491
20% porous	1st	0.615	9.203	0.419	9.987	9.172	0.815
	2nd	0.615	9.204	0.615	10.099	9.184	0.915
30% porous	1st	0.922	8.053	0.449	8.987	7.967	1.020
	2nd	0.492	4.295	0.230	4.726	4.190	0.536
	3rd	0.502	4.309	0.317	4.758	4.184	0.574
40% porous	1st	0.658	3.697	0.220	4.421	3.771	0.650
50% porous	1st	0.820	3.068	0.194	3.786	2.984	0.802
	2nd	0.850	3.111	0.219	3.877	N/A	N/A
	3rd	0.825	3.087	0.195	3.899	3.052	0.847

Some of the produced samples with dense and porous architecture are listed with important production process stages in Table 6. Thirteen different green specimens in total (three dense, one 10% porous, two 20% porous, three 30% porous, one 40% porous and three 50% porous specimens) are sintered with the procedures explained in the previous chapter. Producing a non-oxidized and homogenous porosity structured specimens depends on many parameters, therefore all of these measures are listed in this table.

The production process includes 3 main stages which are: 1) mixing and compacting the powders (green sample phase), 2) conventional sintering and 3) cooling the sample to room temperature. Different experimental parameters were taken into account in these steps. In the 1st stage, the mixing duration, PVA solution concentration, contamination possibility and waiting period of the compacted powder were noted for every specimen. For the sintering stage, argon level in tube, air permeability of the furnace and contamination possibilities were observed. In addition to measurements in the sintering stage, the temperatures where the samples were exposed to atmosphere in and out of the furnace were noted for the cooling stage, as well as the location of specimens during the cooling.

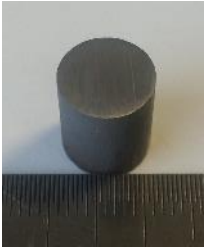

Table 6 Comparison of the production processes of some specimens


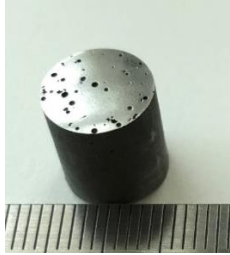
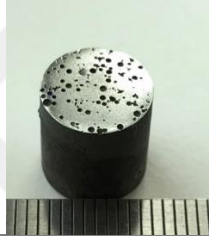
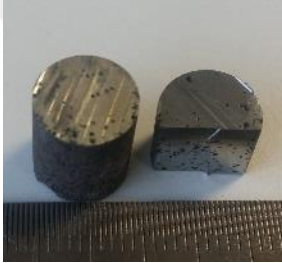


Production Phase	Production Phase Observations	Dense		10% porous	20% porous		30% porous			50% porous	
		1st	2nd	1st	1st	2nd	1st	2nd	3 rd	1st	2nd
Mixing and Compacting Green sample	Mixing duration	15 min	15 min	30 min	15 min	40 min	15 min	30 min	30 min	30 min	15 min
	Concentration level of PVA solution	2.5 % of distilled water	3.6% of distilled water	Unknown	Unknown	2.5 % of distilled water	Unknown	2.5 % of distilled water	3.6% of distilled water	2.5 % of distilled water	3.6% of distilled water
	Mg addition as oxygen getter	0.5 g	0.6 g	0.4 g	0.3 g	0.2 g	0.2 g	0.2 g	0.32 g	0.1 g	0.1 g
	Contamination	None known	None known	Mixed twice with powder addition	None known	None known	None known	None known	None known	None known	None known
	Waiting duration before CS	16 h	15 h	17 h	22 h	16 h	18 h	14 h	16 h	13 h	12 h
Conventional Sintering (5 hours)	Argon level	Above 50 kPa	Below 50 kPa	Above 50 kPa	Above 50 kPa	Above 50 kPa	Above 50 kPa	Above 50 kPa	Below 50 kPa	Above 50 kPa	Below 50 kPa
	Air permeability	OK	OK	OK	OK	OK	OK	OK	OK	OK	OK
	Contamination	Rubber plug was burnt during CS	None known	None known	None known	None known	Sintered without the outer lid	None known	None known	None known	None known
Cooling period (8 hours)	Argon level	Above 50 kPa	Below 50 kPa	Above 50 kPa	Above 50 kPa	Above 50 kPa	Above 50 kPa	Above 50 kPa	Below 50 kPa	Above 50 kPa	Below 50 kPa
	Air permeability	OK	OK	OK	OK	OK	OK	OK	OK	OK	OK
	Location of specimen	Below cooling zone	Cooling zone	Cooling zone	Cooling zone	Cooling zone	Cooling zone	Cooling zone	Cooling zone	Cooling zone	Below cooling zone
	T argon feed is closed	Below 60°C	Below 60°C	590°C furnace T	590°C furnace T	400°C furnace T	660°C furnace T	300°C furnace T	Below 60°C	Below 60°C	310°C furnace T
	T exposed to atmosphere	Below 60°C	Below 60°C	Below 60°C	Below 60°C	Below 60°C	Below 60°C	Below 60°C	Below 60°C	Below 60°C	Below 60°C






In Table 7, digital images of all produced specimens with their macroscopical investigations are listed according to the desired porosity levels. As it can be seen from this table, two of the samples (one dense and one 50% porous specimens) were highly oxidized after sintering phase and three of them (one 20% porous and one 30% porous specimens) had very poor pore distribution along the diameter and the length. The oxidization of two specimens can be the result of poor atmosphere control of the sintering chamber due to the low pressure level of the argon gas.

The poor pore distribution can be due to the inhomogeneous powder mixture before sintering or unsuccessful vaporization of magnesium during sintering. The other common measurement noted during the production of these specimens before sintering was the PVA concentration level used in the mixing which is between 2.5% to 3.6% weight in distilled water. This amount was dictated according to the previous studies, hence further investigation with different concentration levels were analyzed.

Table 7 Digital Images of the produced specimens

Porosity Level	Specimen No	Visual Diagnosis	Image
Dense	1 st	Variable diameter because green sample was partially damaged	
	2 nd	Extremely oxidized and combined with MgO pellet during CS, Removed from MgO pellet by force and additional on-purpose oxidization	

	3rd	OK macroscopically	
10% porous	1st	OK macroscopically	
20% porous	1st	OK macroscopically	
	2nd	Poor pore distribution (macroscopically)	
30% porous	1st	OK macroscopically	
	2nd	Poor pore distribution (macroscopically)	

	3 rd	OK macroscopically (MgO formation only on surface)	
40% porous	1 st	OK macroscopically	
50% porous	1 st	OK but slightly poor pore distribution	
	2 nd	Highly oxidized	
	3 rd	OK macroscopically	

To sum up, eight out of thirteen specimens produced are macroscopically found appropriate for further characterization.

4.2. Thermal Characterization

Differential scanning calorimetry analyses are conducted on macroscopically appropriate specimens. During cutting process of DSC samples, low cutting speeds have been applied and these samples are taken from the outer part of specimens (the most stress-free region). Some of the samples did not show any phase transformation in DSC experiments. The reasons for not observing phase transformation in DSC can be oxidation, failure of sintering due to oxidization as well as some other reasons like contamination and unavoidable deformation (although slow cutting speeds are applied in order to avoid stress formation) during preparation of samples.

In Figure 22, DSC curves of the specimens which have 0% (bulk), 10%, 20%, 30% and 40% porosity levels are shown. The heat flow data are divided into the masses of the samples, such that normalized heat flow is shown on the DSC graphics for every samples. As it can be seen from the figure, all five selected specimens exhibit phase transformation during heating and cooling stages.

There is no reason to have relationship between the change in phase transformation temperature and porosity levels; since the magnesium amounts added during the sintering are kept constant for every specimen by placing additional magnesium powders in specimen holder. However, oxidation is always a problem if the conventional sintering is the main step in the powder metallurgy. Hence, the change in the transformation temperatures can be the result of stress formation during cutting, precipitation formation and chemical inhomogeneity which are present although precautions applied to avoid them.

10% and 20% porous specimens show more than one peak during austenite phase transformation since the chemical inhomogeneity may lead to the formation of secondary phases or intermetallic such as Ti_3Ni_4 and $TiNiO$ during the atomization process of the NiTi prealloyed powder as well as during sintering stage.

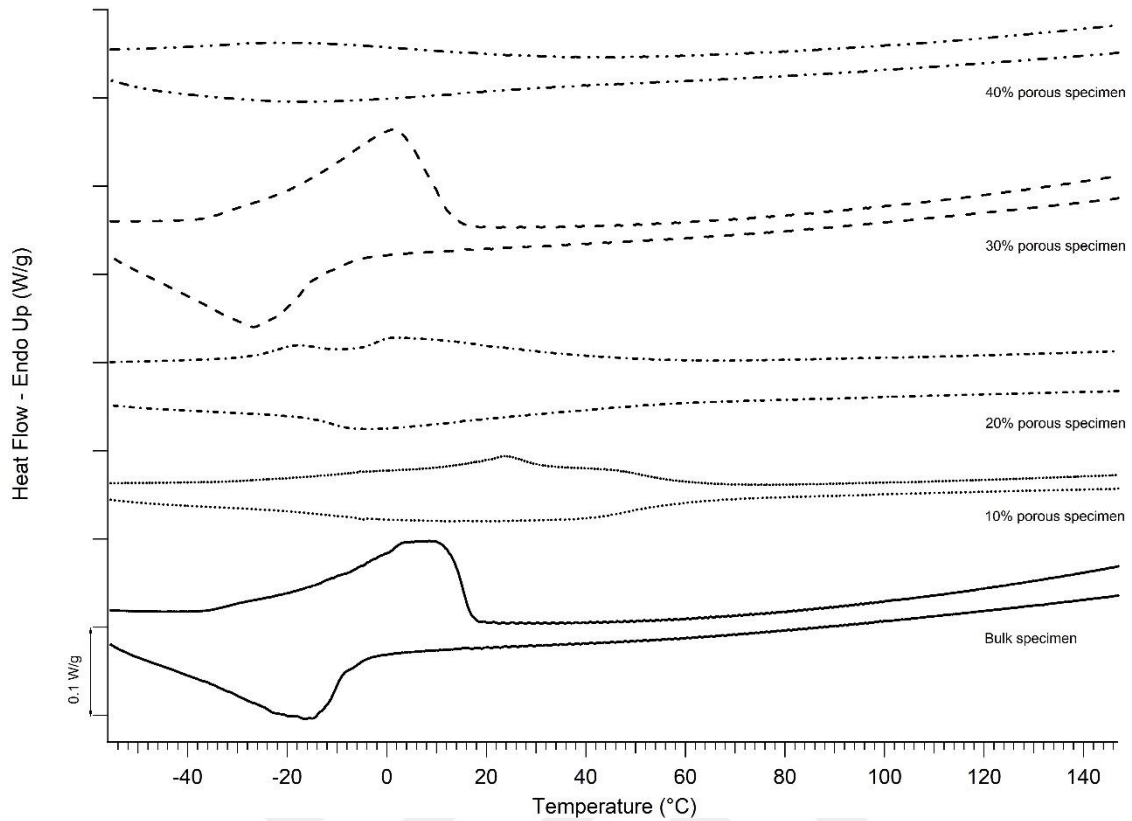


Figure 22 Comparison of DSC heating and cooling curves of pre-alloyed NiTi specimens sintered 1 hour at 1100°C and 2 hours at 1200°C, with different porosity levels

The values of the transformation temperatures are given in Table 8.

Table 8 Phase transformation temperatures of specimens

Specimen	M_f	M_s	A_s	A_f
Bulk	- 55.30	- 1.20	- 25.20	22.70
10% porous	- 24.00	58.90	- 1.20	62.40
20% porous	- 16.30	49.00	- 9.00	51.00
30% porous	- 47.00	- 12.40	- 26.70	14.37
40% porous	- 60.00	21.00	- 44.80	42.10

The comparison of austenite and martensite phase transformation temperatures of all samples is shown in Figure 22. Although there are exceptions, there is a tendency for decreasing phase transformation temperatures with increasing

porosity levels in overall. As it is stated before, there is no evidence for direct impact of porosity levels on transformation temperatures but the reason might be the easiness of oxidation in the specimens with higher porosity amounts (due to having more exposed surface area) during the cooling process. The argon atmosphere together with evaporating powder should decrease the partial pressure of oxygen in the furnace such that oxidation can be minimized. Additionally, titanium sponges are placed in the setup for avoiding further oxidization, however, this amount of oxidization might still not be avoidable.

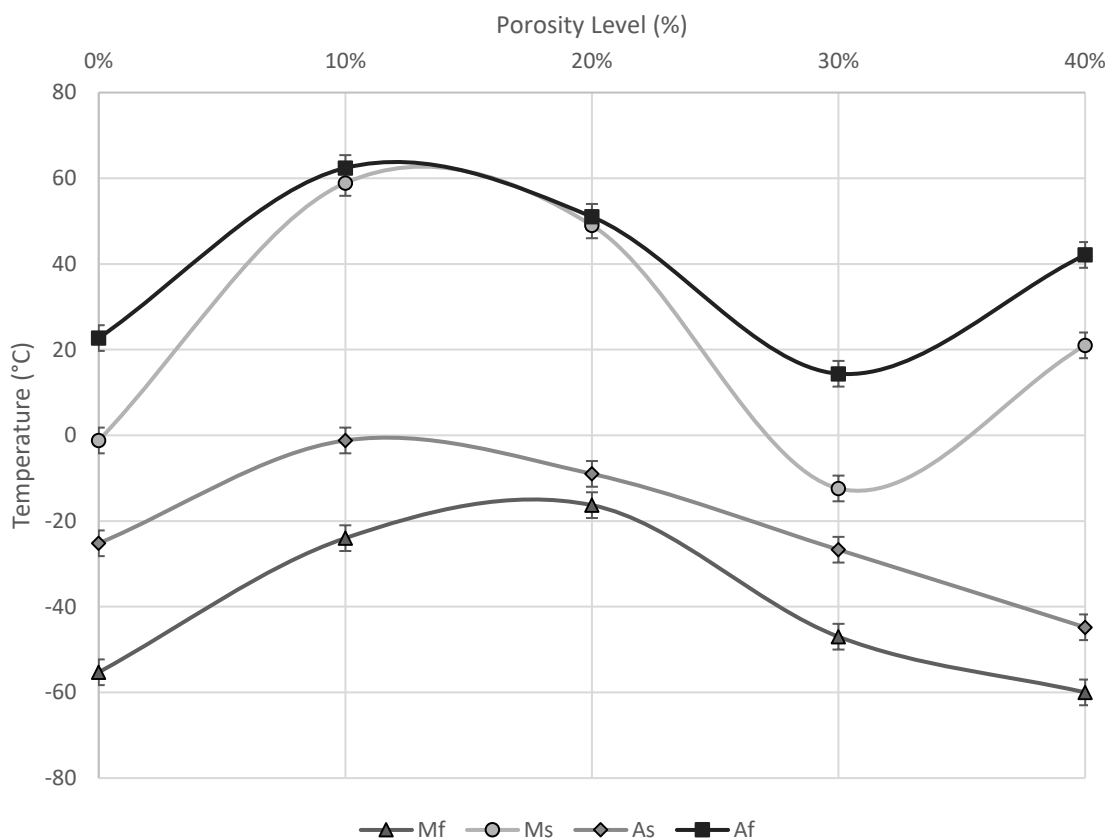


Figure 23 Comparison of phase transformation temperature of specimens

4.3. Structural Characterization of Specimens Produced

4.3.1 Porosity Levels and Distribution

In Figure 24, images obtained from the optical microscope for specimens of bulk, 10%, 20%, 30% and 40% porous specimens can be seen. The obtained pores with magnesium space holder technique, have been preserved the round shape of magnesium particles due to the optimized compression pressure of 400 MPa applied to form green samples. The pore distribution is observed to be more homogenous compared to other porous NiTi specimen production methodologies in literature.

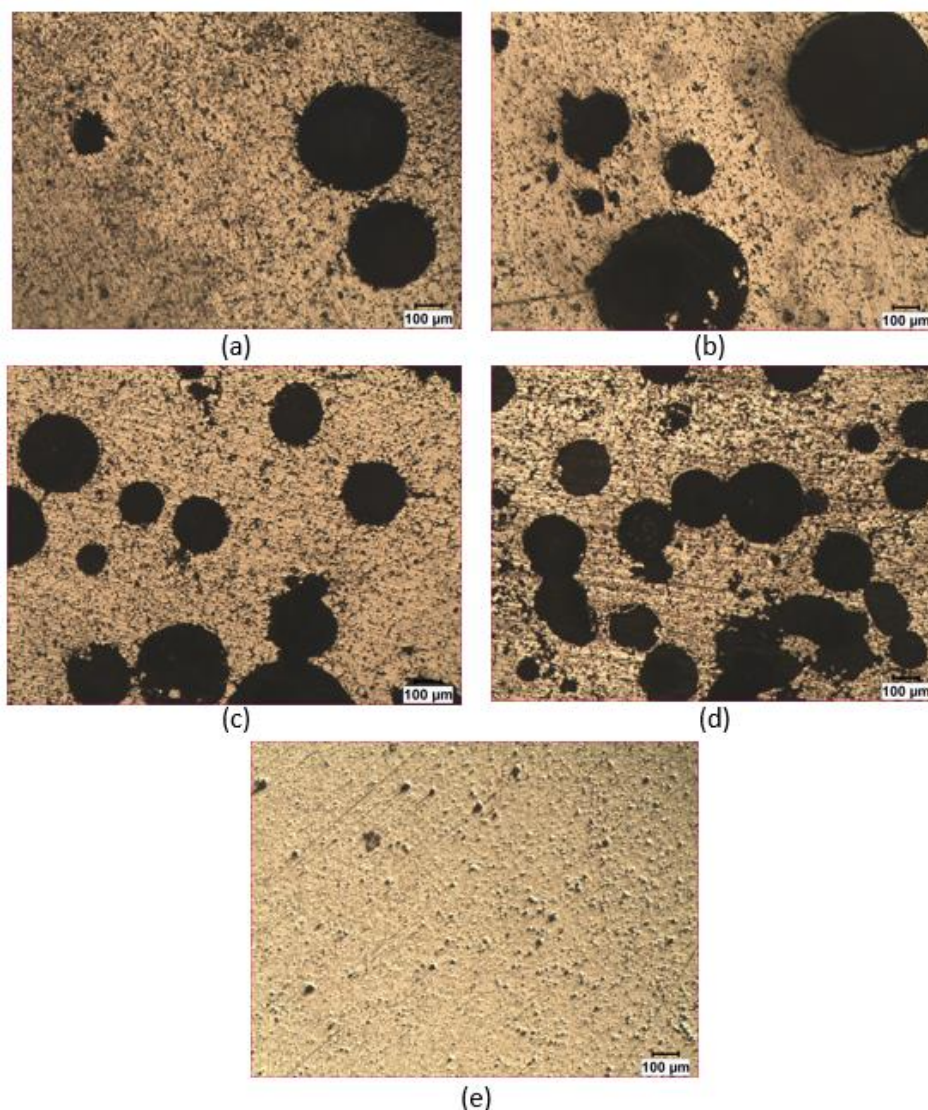


Figure 24 Optical microscope images after grinding and polishing of (a) 10% porous specimen, (b) 20% porous specimen, (c) 30% porous specimen, (d) 40% porous specimen and (e) bulk specimen

The macro-porosity percentages calculated from the images for each specimens are given in the Appendices section of this thesis. Between ten to fifteen different images are captured from different areas of specimens' surfaces. In these analyses, micro-porosities are neglected since the resolution of the optical microscope is not enough to determine the micro-porosities in the samples.

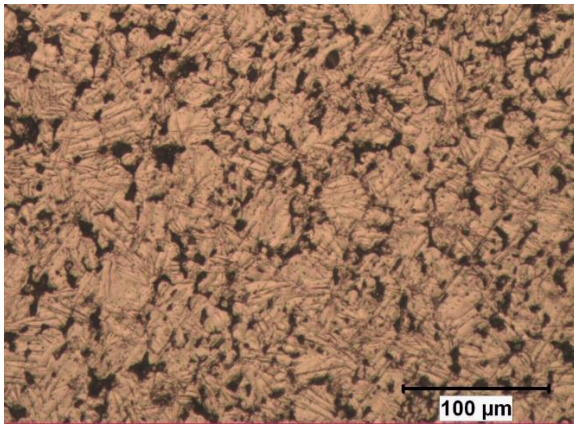
The macro-porosity levels of the specimens are calculated with the image analyses tool of the optical microscope and are shown in Table 9. The macro-porosity show consistent increase with the volumetric magnesium addition.

Table 9 Macro-porosity amounts of specimens

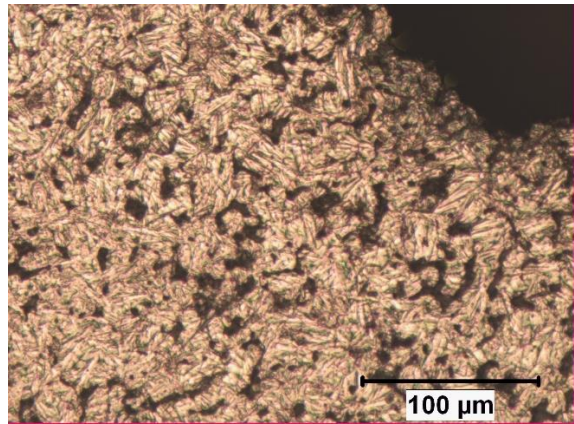
Mg Addition (vol.)	Macroporosity Levels (optical microscope)
0%	
10%	14.2%
20%	19.6%
30%	30.8%
40%	50.3%

4.3.2 Micrographs of the Specimens

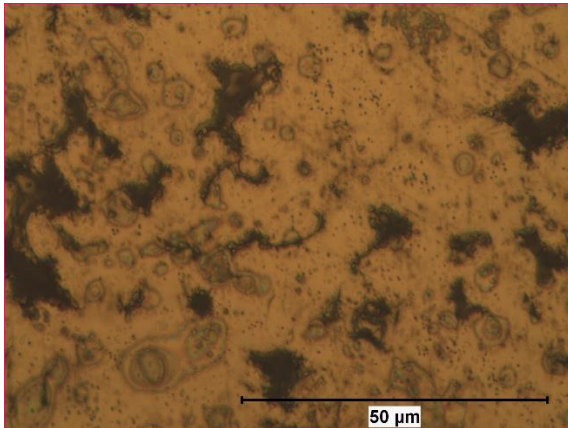
In Figure 25, images of the five specimens are shown, which are obtained by optical microscope after application of etching on the surfaces. In (a) and (b), 10% and 20% porous specimens are shown at room temperatures, both martensite and austenite phases are observed as it is expected from the DSC results. On the other hand, only austenite phase has been observed in other specimens.



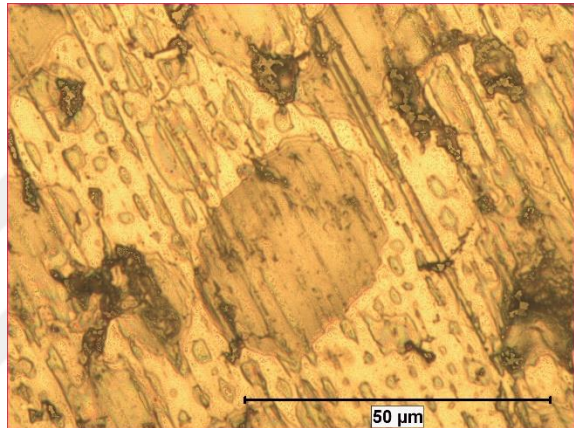
(a) %10 porous



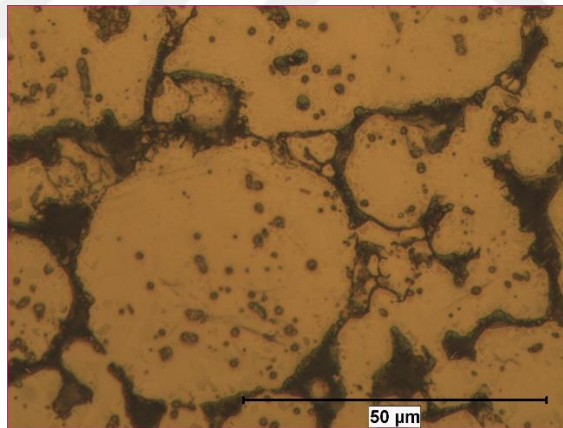
(b) 20% porous



(c) 30% porous



(d) 40% porous



(e) Bulk

Figure 25 Optical microscope images after etching of (a) 10% porous specimen (martensite exists at RT), (b) 20% porous specimen (martensite exists at RT), (c) 30% porous specimen (no martensite at RT), (d) 40% porous specimen (no martensite at RT) and (e) bulk specimen (no martensite at RT)

4.4. The Superelasticity Behavior of Specimens

The compression tests are completed for selected five specimens, which are produced with 0%, 10%, 20%, 30% and 40% porosity levels. The specimens are loaded up to 3% strain at different temperatures starting from $M_s + 15$ or $M_s + 45$, depending on the martensite start temperature of the specimens and with increments of 30 and 40°C up to 450 °C. The main goal of these experiments is to observe M_d temperature for each specimens having different porosity levels. The exact temperature levels for every specimen can be seen in Table 10.

Table 10 Compression Tests Temperature Levels for Every Specimen

Temperature	Bulk	10% Porous	20% Porous	30% Porous	40% Porous
M_s (°C)	-1	59	49	-12	21
$M_s +15$ (°C)	-	74	64	-	-
$M_s +45$ (°C)	44	104	94	33	66
$M_s +75$ (°C)	74	134	124	63	96
$M_s +105$ (°C)	104	164	154	93	126
$M_s +135$ (°C)	134	194	184	123	156
$M_s +165$ (°C)	164	224	214	153	186
$M_s +195$ (°C)	194	254	244	183	216
$M_s +235$ (°C)	234	294	284	223	256
$M_s +275$ (°C)	274	334	324	263	296
$M_s +315$ (°C)	314	374	364	303	336
$M_s +355$ (°C)	354	414	404	343	376
$M_s +395$ (°C)	394	454	444	383	416
$M_s +435$ (°C)	434	-	-	423	456
$M_s +475$ (°C)	-	-	-	463	-

Additionally, first cycle effect is tested with bulk and 30% porous specimens at three different temperatures selected (M_s+45 , M_s+275 and M_s+335) for 5 cycles because there are several references to referring to the first cycle effect which is generally observed in NiTi alloys. The superelasticity behavior of the NiTi alloy during the first cycle loading and the second cycle loading is not same [39]. Similarly, it is stated in the study of Zhang et al that superelasticity behavior is observed again and preserved after first cycle of a Ti-50.8 at Ni specimen with %27 porosity [14].

4.4.1 Superelasticity Behavior with Temperature

Five different sintered NiTi (Ni-49.6 at. %Ti content) specimens (bulk, 10%, 20%, 30% and 40% porous) were tested by applying 3% strain magnitude with increasing temperature at every cycle. The tests were started at least 15°C above the martensite start temperature in order to observe their superelastic behavior. There are two requirements for superelasticity in shape memory alloys which are:

1. The critical stress for slip should be lower than the critical stress to induce martensite.
2. The test temperature should be above austenite finish temperature of the specimen. [40]

In order to describe the compressive superelastic behavior of porous NiTi specimens, one cycle conducted on 20% porous specimen at 124°C has been selected and shown in Figure 26. It should be noted that almost all of the specimens demonstrated the similar stress-strain behavior in the superelastic temperature interval.

During loading, three different stress stages are observed;

- Firstly, the specimens show exponentially increasing stress magnitude which is the result of porous structure. In this stage, porous structure starts to deform by loading.
- Then, linear stress increase is observed due to the elastic deformation of austenite phase.
- After the elastic deformation vanishes, critical stress level to induce martensite is reached and the martensite phase transformation starts with the increase in stress.

During unloading, two different stress curves are obtained as follows:

- Firstly, again a linear stress decrease occurs due to elastic strain recovery of the martensite.
- Then the reverse transformation starts and almost all of the strain is recovered.

Although strain recovery was obtained in all of the specimens between A_f and M_d temperatures, there was always some unrecovered strain left in all tests and at all temperatures. It should also be the result of porous structure, because the critical stress to slip level is reached around the sintering necks and plastic deformation starts at some of the local regions of porous specimens. In addition to these, the bridges in between the macro-pores should be exposed to different stress and strain levels. The martensite regions that has been plastically deformed, does not transform into austenite due to dislocations formed at interfaces of austenite and martensite plates. It should be also noted that same specimens (not virgin) were used for same porosity level at every test temperature. Therefore, the residual strain can be also a result of repetitive loading to same specimen, due to dislocations formed at previous tests.

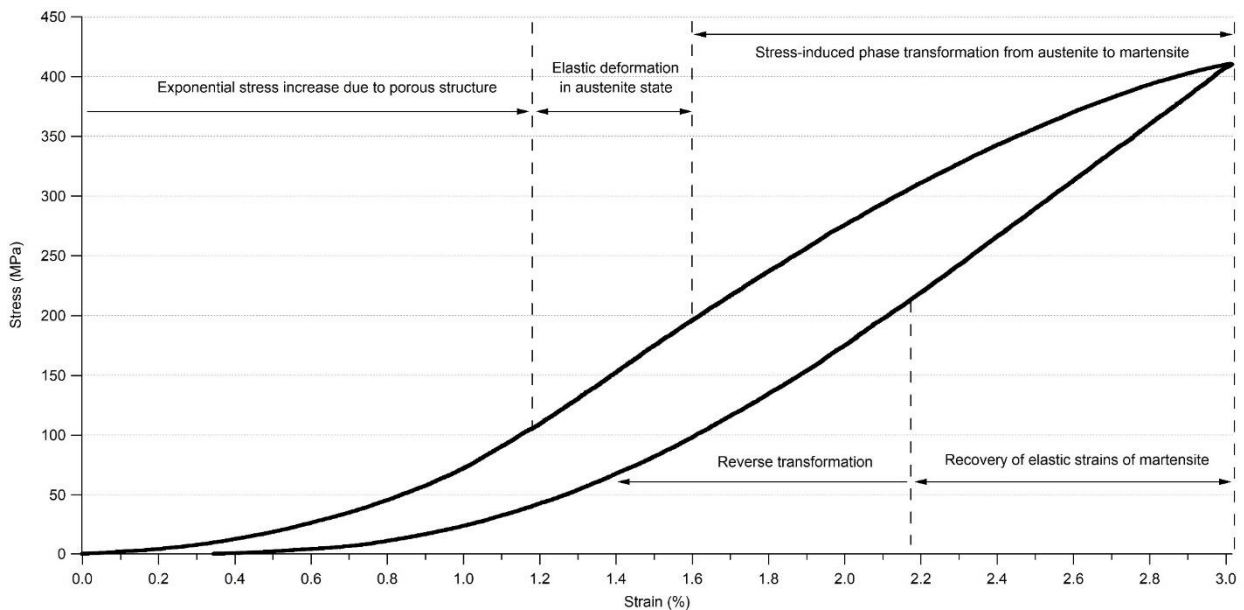


Figure 26 Superelasticity behaviour of 20% porous specimen at 124°C, between A_f and M_d (selected for description)

The loading and unloading compression test results are given starting from Figure 27 to Figure 31 for specimens with 0%, 10%, 20%, 30% and 40% Mg addition, respectively.

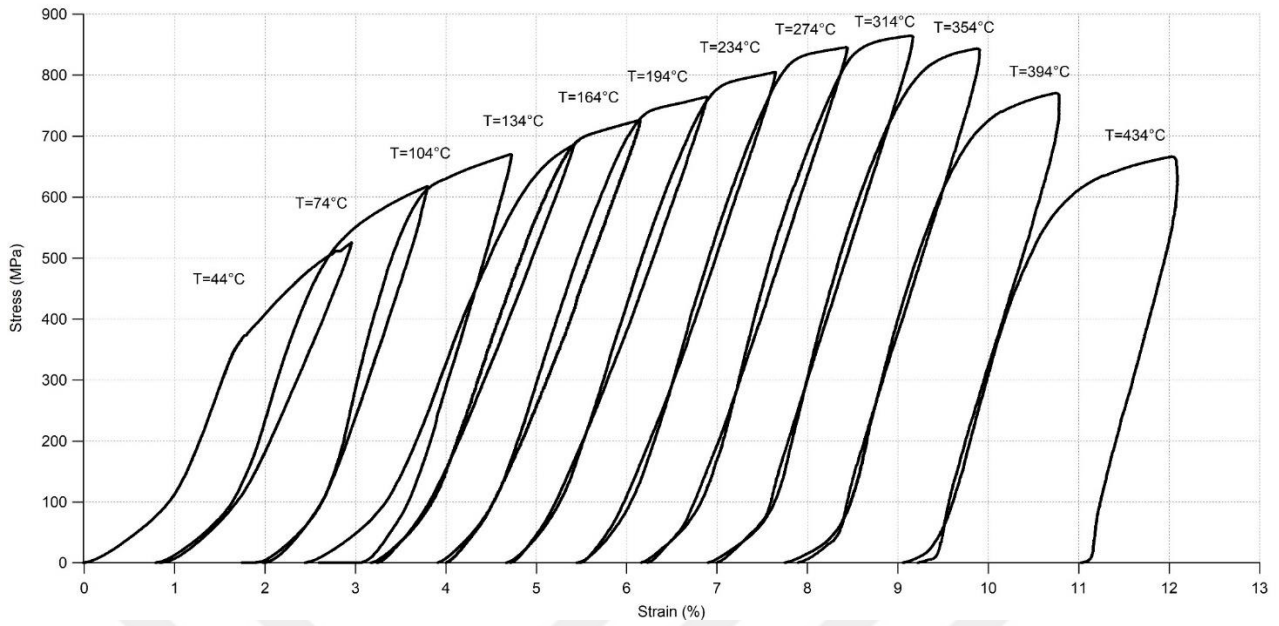


Figure 27 Stress-strain diagram of bulk specimen compressed to 3% strain level at different temperatures

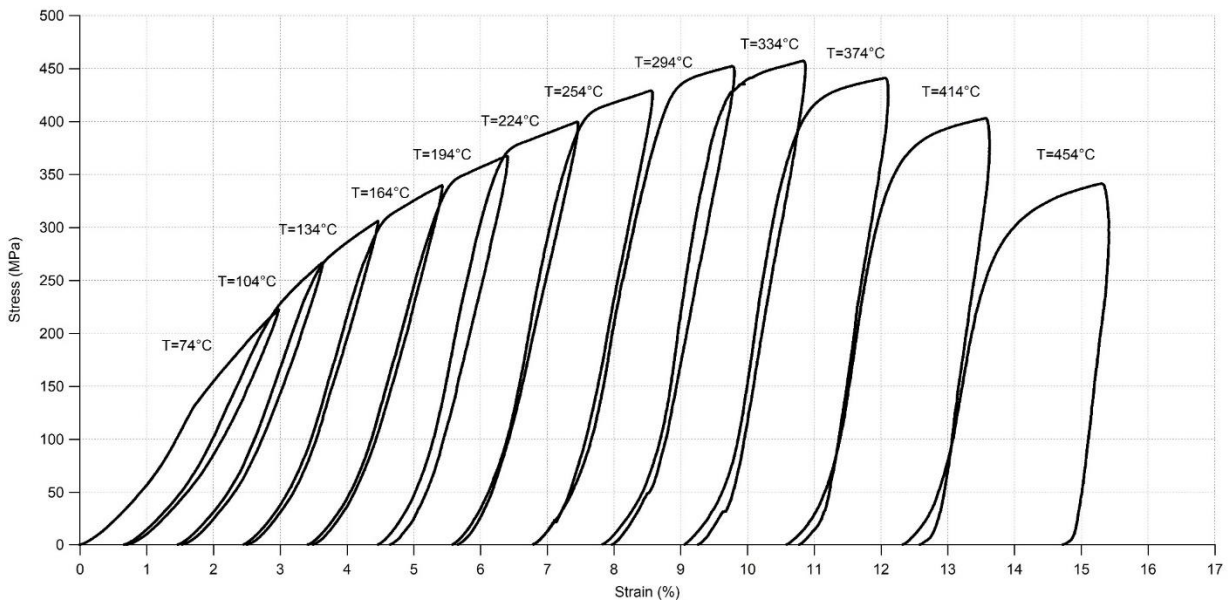


Figure 28 Stress-strain diagram of 10% porous specimen compressed to 3% strain level at different temperatures

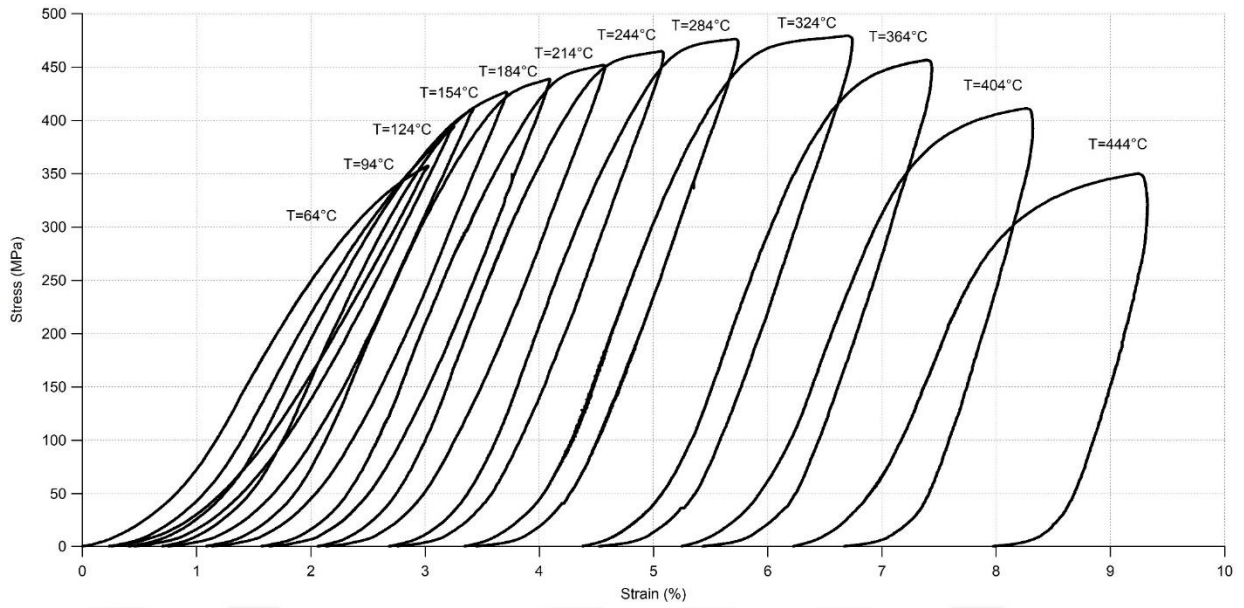


Figure 29 Stress-strain diagram of 20% porous specimen compressed to 3% strain level at different temperatures

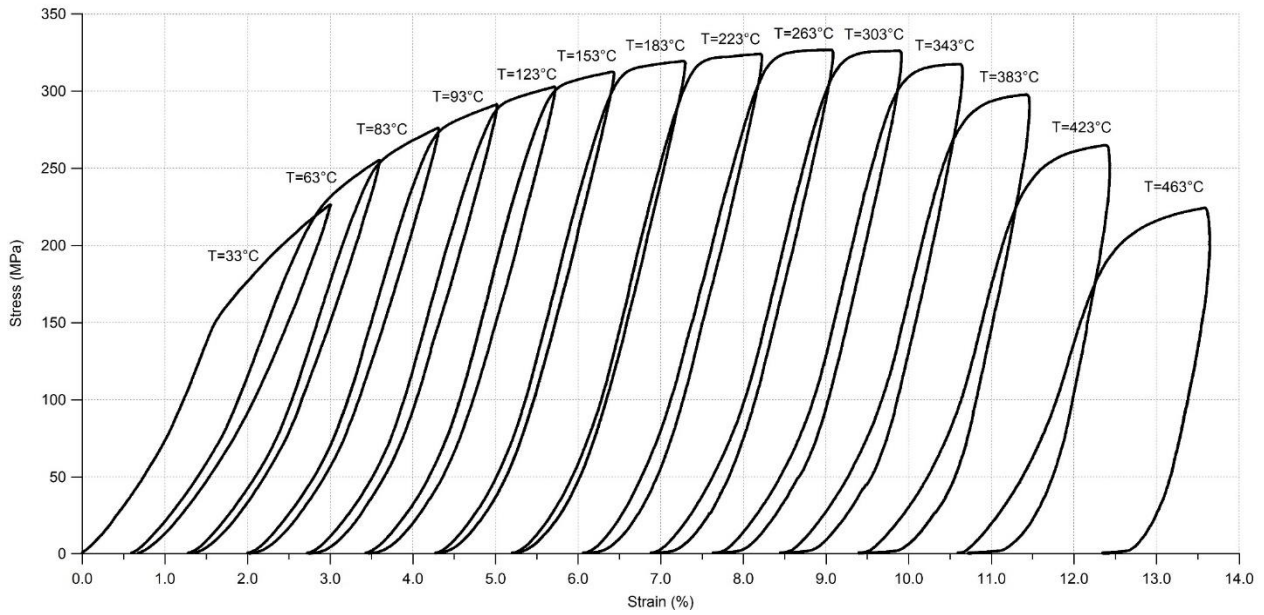


Figure 30 Stress-strain diagram of 30% porous specimen compressed to 3% strain level at different temperatures

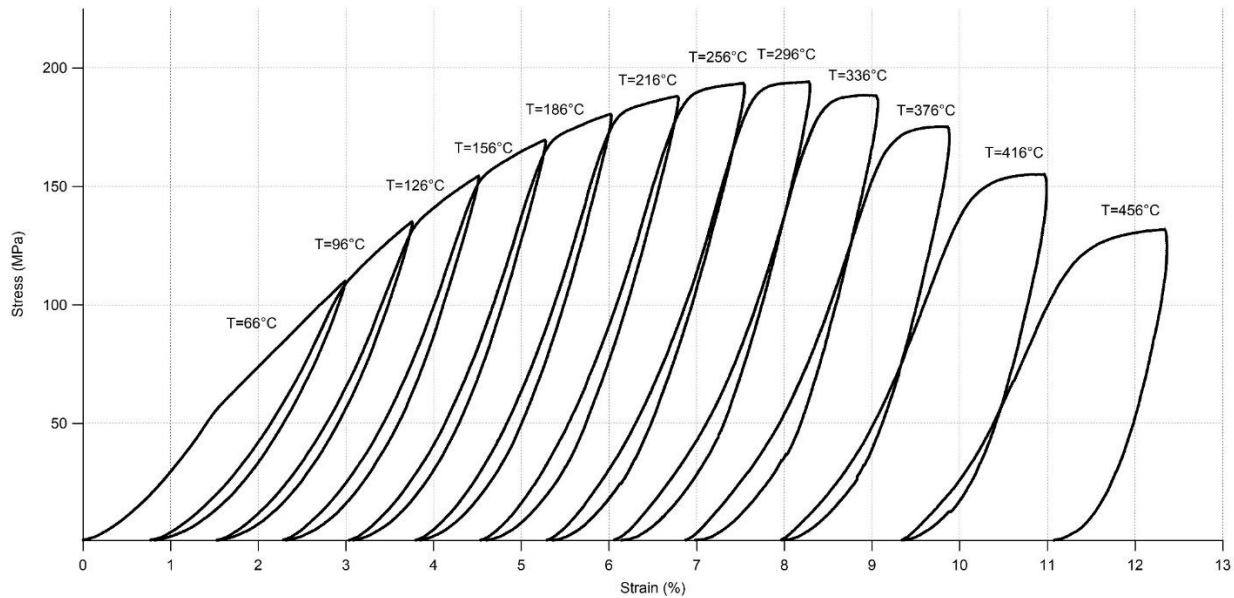


Figure 31 Stress-strain diagram of 40% porous specimen compressed to 3% strain level at different temperatures

According to these figures; general discussions can be summarized as below:

- The strength and critical stress to induce martensite levels increase with increasing temperature for all specimens up to a temperature level which is the maximum temperature to induce martensite. Because higher stress levels are required to obtain austenite to martensite transformation at higher temperatures.
- Above M_d temperature, irrecoverable strain amounts increase significantly and lower strength is observed for every specimen.

Bulk specimen has been reached 860 MPa stress during these tests which is the highest level among all specimens as expected. The highest stress level is obtained at 314°C ($M_s+315^\circ\text{C}$) as it can be seen from Figure 27. The reverse transformation almost did not occur after this temperature level.

10% Mg added specimen has been reached 460 MPa stress at maximum during these tests. The highest stress level is obtained at 334°C ($M_s+275^\circ\text{C}$) as it can be seen from Figure 28. Similar to bulk specimen, the reverse transformation almost did not occur after this temperature level.

20% Mg added specimen has reached to 480 MPa stress at maximum during these tests which is a little higher than that of 10% Mg added specimen. The highest stress level is obtained at 324°C ($M_s+275^\circ\text{C}$) as it can be seen from Figure 29.

30% Mg added specimen showed maximum 325 MPa stress level during these tests. The highest stress level is obtained at 263°C ($M_s +275^\circ\text{C}$) as it can be seen from Figure 30.

40% Mg added specimen reached to 190 MPa stress during these tests which is the lowest level among all specimens as expected. The highest stress level is obtained at 296°C ($M_s +275^\circ\text{C}$) as it can be seen from Figure 27.

Additionally, in order compare the superelastic behavior of specimens at the same temperature levels with respect to phase transformation temperatures, $M_s + 75^\circ\text{C}$ (below M_d) and $M_s +355^\circ\text{C}$ (after M_d) temperatures are selected.

In Figure 32, compression test results of all specimens conducted at 75°C above their martensite start temperature, are illustrated. At this temperature where stress-induced martensite transformation is possible;

- The bulk sample showed the highest strength and stress levels to the same strain deformation and 40% porous samples showed the lowest values, as it is stated before.
- The best strain recovery performance was observed in 20% porous specimen with 2.7% strain recovery and the worst strain recovery was observed in bulk sample with 1.8% strain recovery.
- The stress levels were decreased with increasing porosity levels; however 20% porous specimen demonstrated higher stress levels than 10% porous specimen.

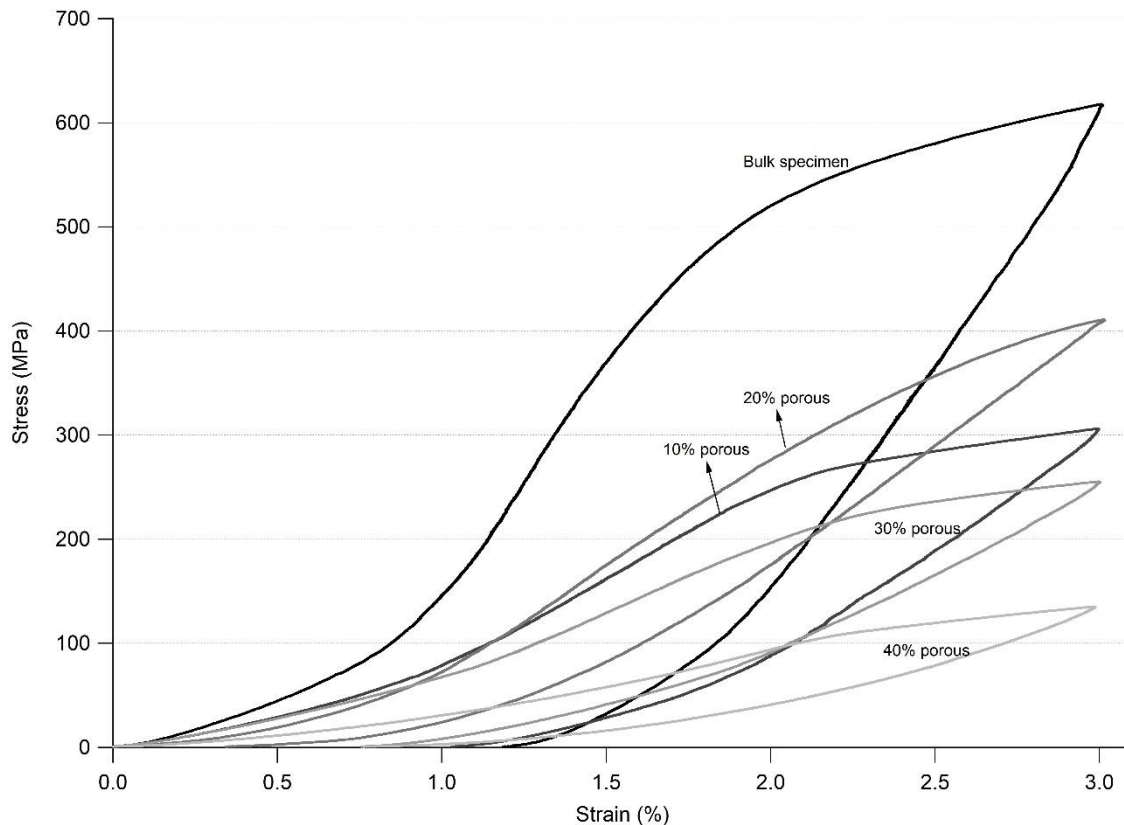


Figure 32 Comparison of stress curves obtained by compression tests conducted at $M_s+75^\circ\text{C}$

In Figure 33, compression test results of all specimens conducted at 355°C above their martensite start temperature, are illustrated. At this temperature where stress-induced martensite transformation is not expected;

- The bulk sample showed the highest strength and stress levels to the same strain deformation and 40% porous samples showed the lowest values similar to previous figure.
- The best strain recovery performance was observed in 30% porous specimen with 2.2% strain recovery and the worst strain recovery was observed in 10% porous sample with 1% strain recovery.
- The stress levels were decreased with increasing porosity levels; however 10% and 20% porous specimens demonstrated similar stress levels.

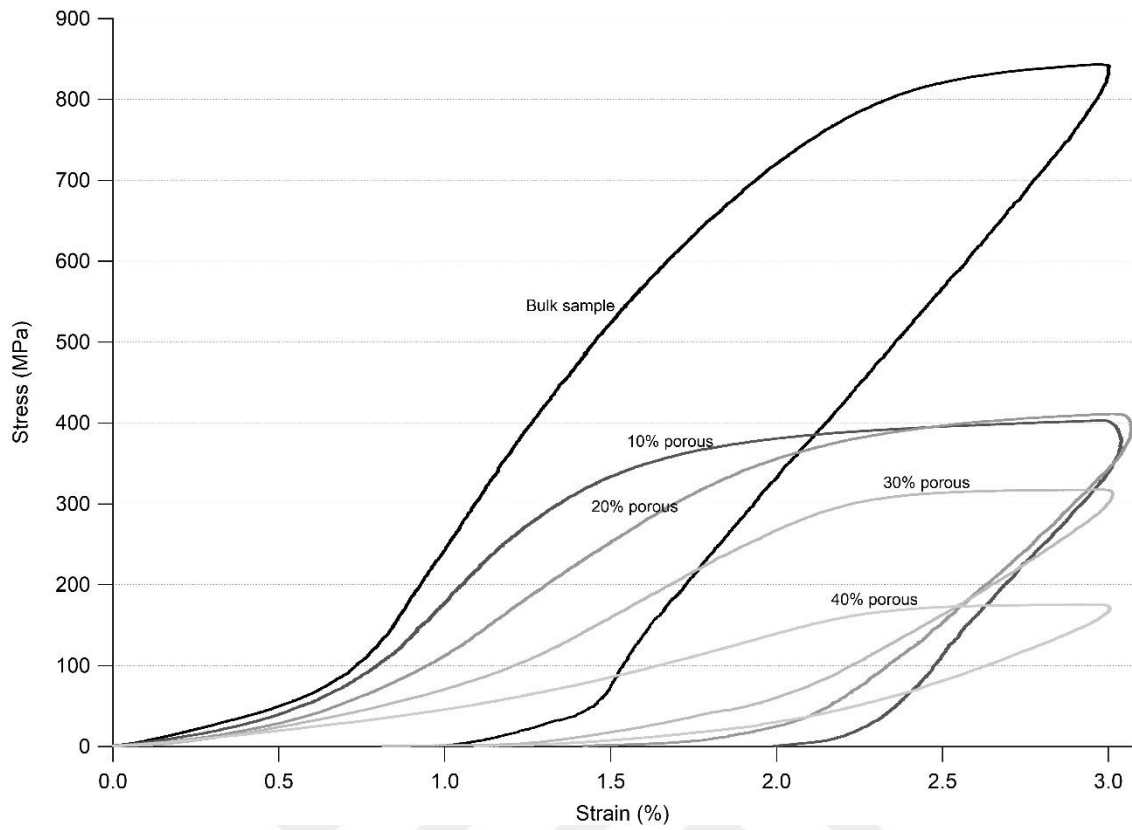


Figure 33 Comparison of stress curves obtained by compression tests conducted at $M_s+355^{\circ}\text{C}$

4.4.2 Critical Stress to Induce Martensite vs Temperature Diagrams

The comparison of the critical stresses to induce martensite (yield strength calculated with 0.2% strain offset method) of porous specimens at different test temperatures can be seen in Figure 34. As expected, specimen with the lowest porosity level, bulk specimen shows the highest stress amount and the specimen with highest porosity levels shows the lowest stress amounts. However, the strength of 10% Mg added specimen was lower than 20% Mg added one. This can be due to higher overall porosity level in 10% Mg added specimen, although there is less macro-porosity observed in optical microscope.

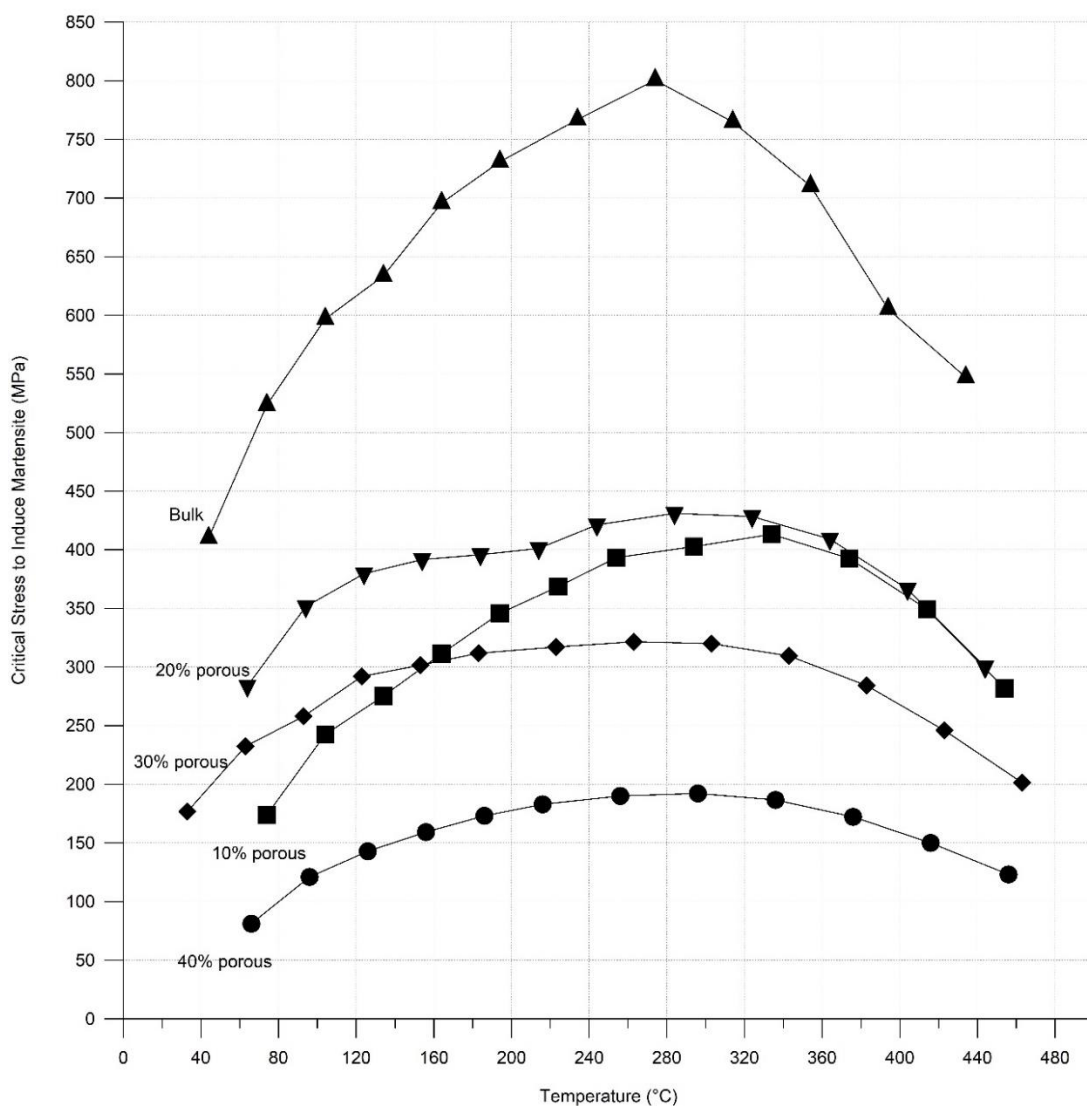


Figure 34 Critical stresses to induce martensite of specimens at different test temperatures

For a more detailed comparison of superelasticity behavior before and after M_d temperature, two loading-unloading curves of 20% porous specimen at 214°C and 454°C are selected and illustrated in Figure 35. In addition to significant decrease

in the strength of the specimen after M_d as discussed earlier, the recovered strain amount before M_d is almost three times larger than that of the cycles after M_d .

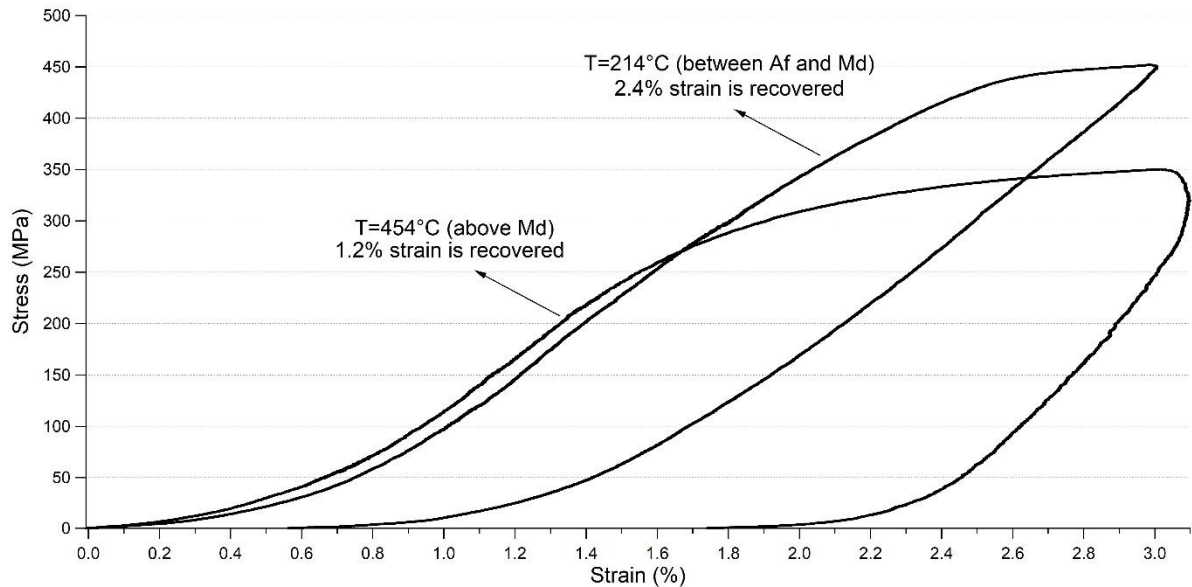


Figure 35 Comparison of the mechanical behavior of 20% porous specimen below and above M_d

Moreover, as it can be seen from Figure 36, the maximum temperature to induce martensite (M_d) point is changing between 250°C and 350°C for porous NiTi specimens in this study. In addition, M_d temperatures of these specimens had been observed at $M_s+275^\circ\text{C}$ in all specimens except 20% porous sample. However, no specific relationship between the porosity level and M_d temperature can be concluded.

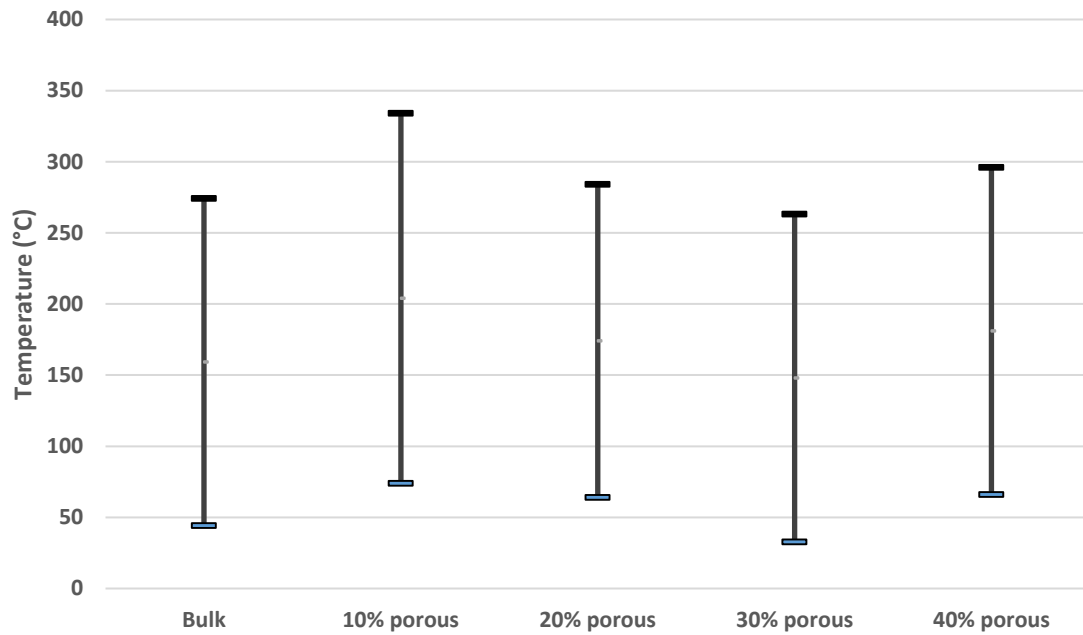


Figure 36 Superelastic temperature window where superelasticity observed for every specimen

On the other hand, the comparison of the maximum temperature to induce martensite obtained from the compression tests and the phase transformation temperatures (M_s and A_f) of the specimens has been made in Figure 37. As it can be seen from this figure, M_d is dependent on the chemical composition of the porous NiTi alloys.

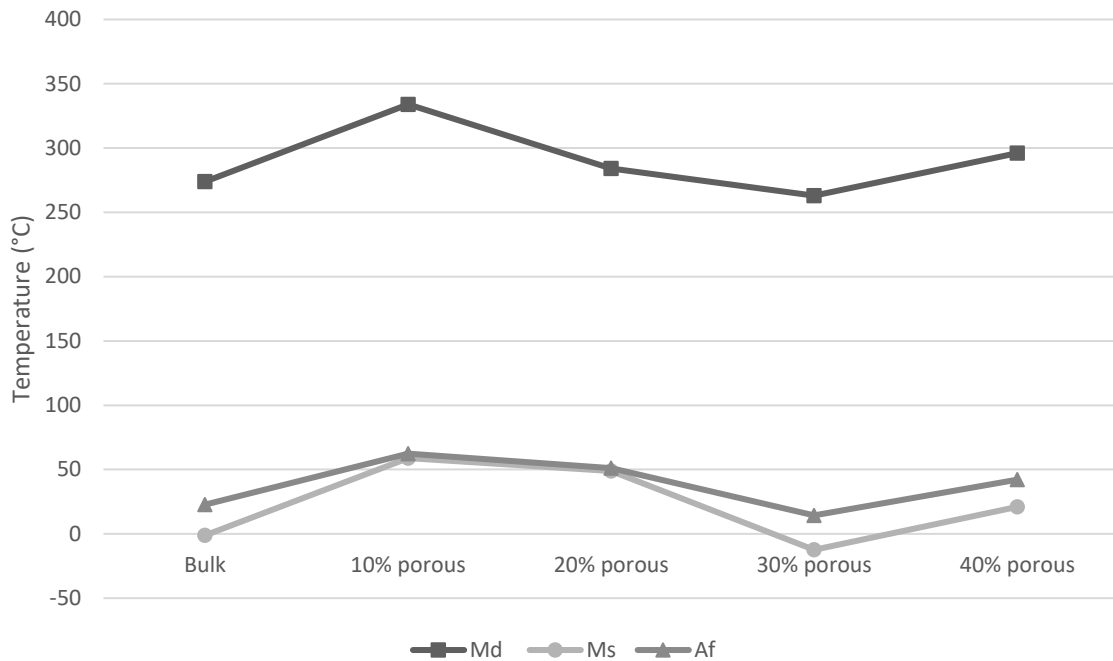


Figure 37 Comparison of phase transformation temperatures with Md

4.4.3 Comparison of Young's Modulus and Irrecoverable Strain Amounts

Modulus of Elasticity of the specimens is calculated from the elastic loading curve of every compression tests conducted. The comparison of values for every specimen can be seen in Figure 38. Although there are some exceptions, it can be said that the modulus of elasticity of every specimen increases with increasing temperature until approximately M_d and then starts to decrease. This also emphasizes that after M_d temperature, shape memory alloys starts to behave like conventional metals and elasticity of modulus starts to decrease with increasing temperature. As expected the stiffness has a similar pattern with the critical stress to induce martensite.

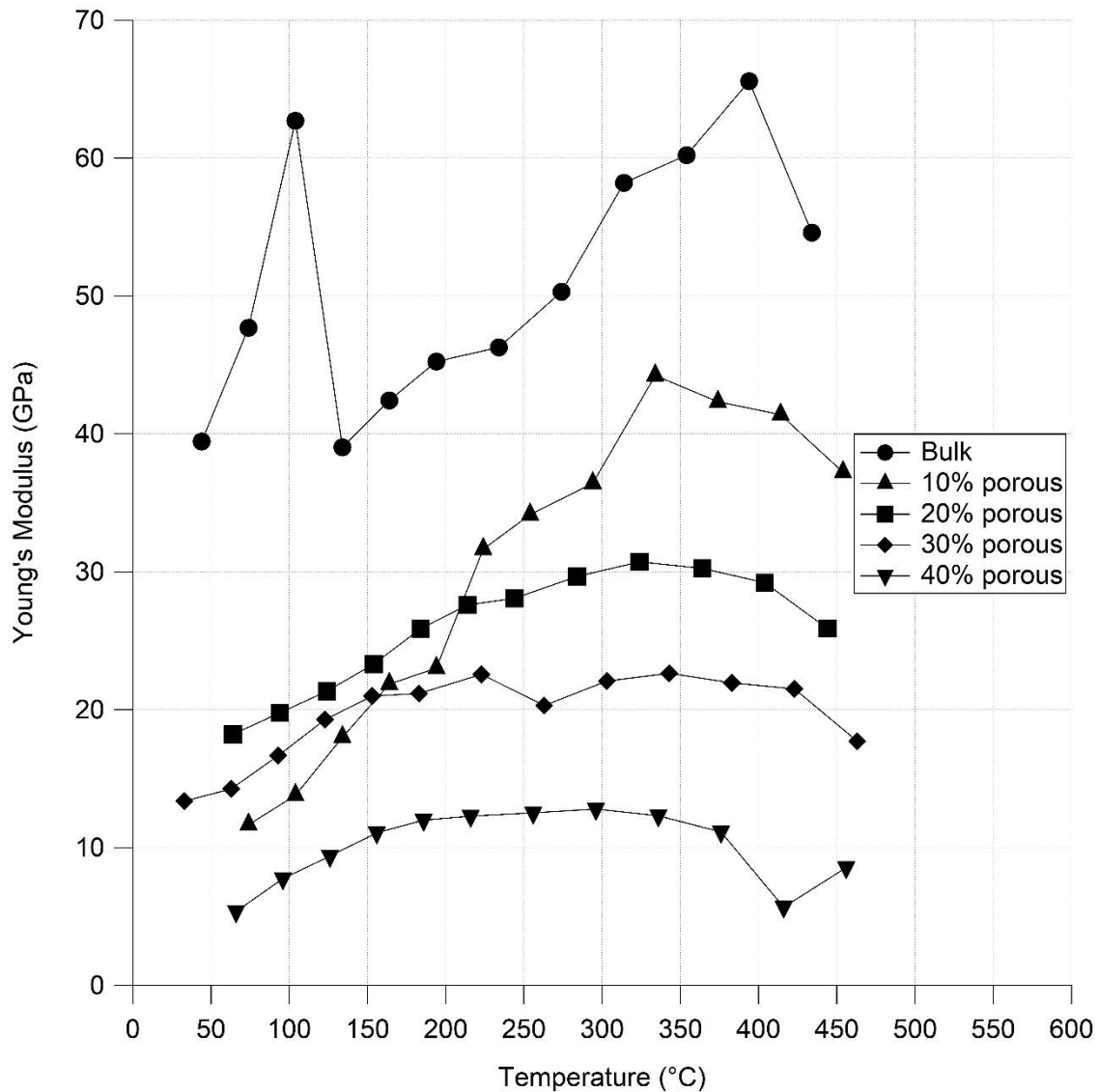


Figure 38 Young's modulus comparison of specimens with respect to temperature

In Figure 39, residual strain amounts are compared for all porous specimens with respect to the test temperatures. The best strain recovery is observed in 20% porous NiTi specimen and the worst behavior is observed in 10% porous one, as it can be seen from the figure. The rest of the specimens almost show the same strain recovery amounts. However, it is clearly apparent that the residual strains are increasing after M_d temperature.

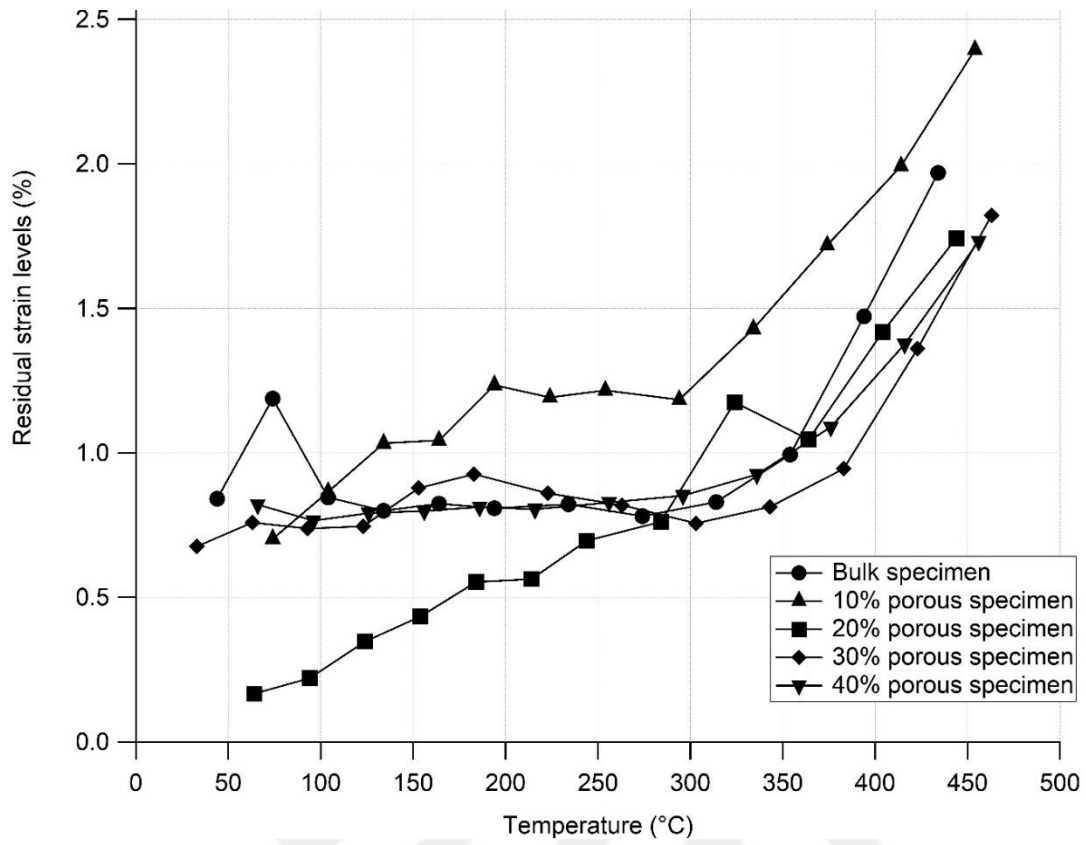


Figure 39 Irrecoverable strain amounts of specimens with respect to test temperatures

5. CONCLUSION

- The porosity amounts and sizes can be controlled easily with the size and amount of magnesium particles added before conventional sintering.
- Phase transformation temperatures (martensite and austenite) does not depend on the porosity amounts; however it is highly depended on the oxidation amounts during sintering and probably other criteria like intermetallic formation.
- There is no observable impact of porosity amounts on the maximum temperature to induce martensite (M_d). It depends on the properties of material not on shape. According to the studied porous and bulk NiTi alloys, M_d point is observed between 260 and 340°C.
- Critical stress to induce martensite increases with decreasing porosity and increasing test temperature, as expected.
- After M_d point, the critical stress to induce martensite and elasticity of modulus decrease, on the other hand the residual strain amounts increase. Hence, it can be said that the superelasticity behavior of porous and bulk NiTi alloys vanishes after M_d point.

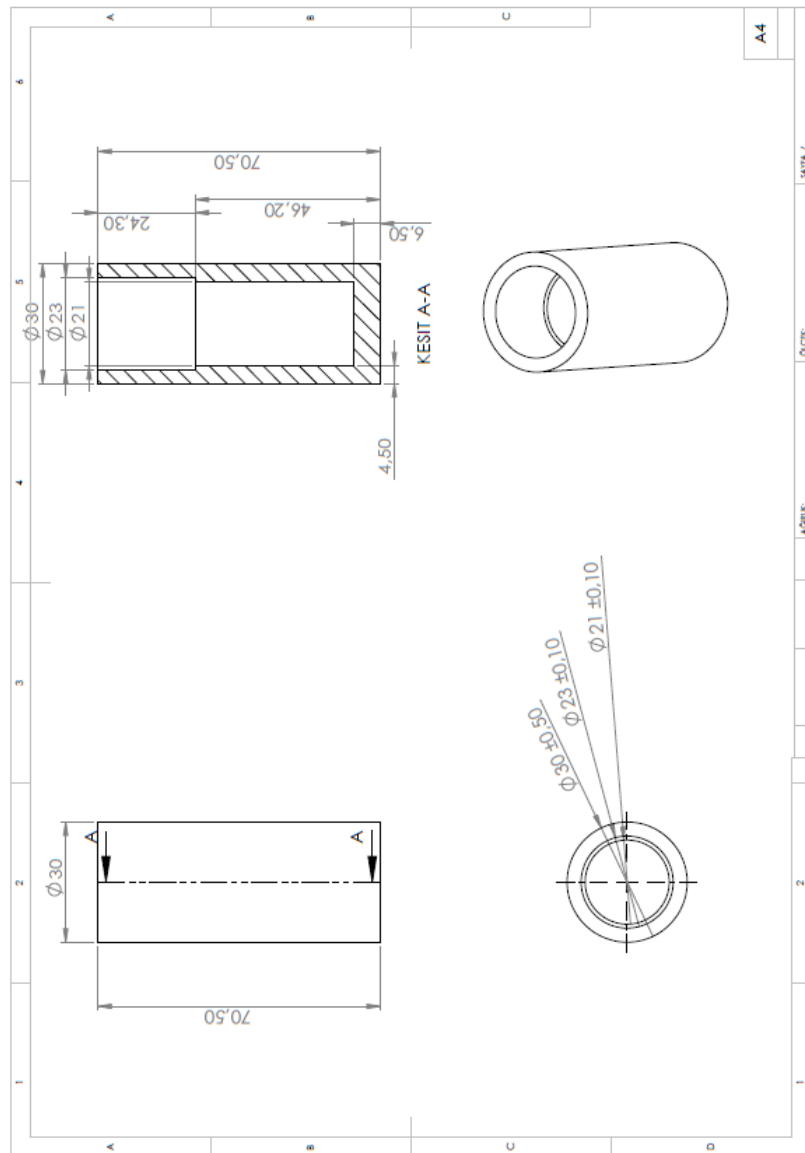
REFERENCES

- [1] Chang, L. and Read, T., Plastic Deformation and Diffusionless Phase Changes in Metals — the Gold-Cadmium Beta Phase, *Journal of the Minerals, Metals and Materials Society*, vol. 3, no. 1, 47–52, **1951**.
- [2] Buehler, W. J., Gilfrich, J. V., and Wiley, R. C., Effect of Low-Temperature Phase Changes on the Mechanical Properties of Alloys near Composition TiNi, *Journal of Applied Physics*, vol. 34, no. 5, 1475–1477, **1963**.
- [3] Brinson, L. C., One-dimensional constitutive behavior of shape memory alloys: Thermomechanical derivation with non-constant material functions and redefined martensite internal variable, *Journal of Intelligent Material Systems and Structures*, vol. 4, no. 2, 229–242, **1993**.
- [4] Lexcelent, C., *Shape-memory Alloys Handbook*. **2013**.
- [5] Yoneyama, T. and Miyazaki, S., *Shape memory alloys for biomedical applications*. **2009**.
- [6] Brunette, D. M., Tengvall, P., Textor, M., and Thomsen, P., *Titanium in Medicine*, vol. 49, no. 0. **2001**.
- [7] Tang, W., Thermodynamic study of the low-temperature phase B19' and the martensitic transformation in near-equiatomic Ti-Ni shape memory alloys, *Metallurgical and Materials Transactions A*, vol. 28, no. 3, 537–544, **1997**.
- [8] Aydoğmus, T., Processing and Characterization of Porous Titanium Nickel Shape Memory Alloys, Middle East Technical University, **2010**.
- [9] Firstov, G. ., Vitchev, R. ., Kumar, H., Blanpain, B., and Van Humbeeck, J., Surface oxidation of NiTi shape memory alloy, *Biomaterials*, vol. 23, no. 24, 4863–4871, **2002**.
- [10] Nishida, M., Wayman, C. M., and Honma, T., Precipitation processes in near-equiatomic TiNi shape memory alloys, *Metallurgical Transactions A*, vol. 17, no. 9, 1505–1515, **1986**.
- [11] Aydoğmuş, T. and Bor, Ş., Processing of porous TiNi alloys using magnesium as space holder, *Journal of Alloys and Compounds*, vol. 478, no. 1–2, 705–710, **2009**.
- [12] Kockar, B., Ozcan, H., and Cakmak, S., Shape memory behavior of Ni-rich NiTi foam with different porosity percentages, *Journal of Intelligent Material Systems and Structures*, vol. 24, no. 9, 1131–1137, **2013**.
- [13] Yuan, B., Chung, C. Y., Huang, P., and Zhu, M., Superelastic properties of porous TiNi shape memory alloys prepared by hot isostatic pressing, *Materials Science and Engineering A*, vol. 438–440, no. SPEC. ISS., 657–660, **2006**.
- [14] Zhang, X. P., Liu, H. Y., Yuan, B., and Zhang, Y. P., Superelasticity decay of porous NiTi shape memory alloys under cyclic strain-controlled fatigue conditions, *Materials Science and Engineering A*, vol. 481–482, no. 1–2 C, 170–173, **2008**.
- [15] Bassani, P., Giuliani, P., Tuissi, A., and Zanotti, C., Thermomechanical properties of porous NiTi alloy produced by SHS, *Journal of Materials*

- Engineering and Performance*, vol. 18, no. 5–6, 594–599, **2009**.
- [16] Zhao, Y., Taya, M., Kang, Y., and Kawasaki, A., Compression behavior of porous NiTi shape memory alloy, *Acta Materialia*, vol. 53, no. 2, 337–343, **2005**.
- [17] Guoxin, H., Lixiang, Z., Yunliang, F., and Yanhong, L., Fabrication of high porous NiTi shape memory alloy by metal injection molding, *Journal of Materials Processing Technology*, vol. 206, no. 1–3, 395–399, **2008**.
- [18] Li, H., Yuan, B., Gao, Y., Chung, C. Y., and Zhu, M., High-porosity NiTi superelastic alloys fabricated by low-pressure sintering using titanium hydride as pore-forming agent, *Journal of Materials Science*, vol. 44, no. 3, 875–881, **2009**.
- [19] Aydoğmuş, T. and Bor, Ş., Superelasticity and compression behavior of porous TiNi alloys produced using Mg spacers, *Journal of the Mechanical Behavior of Biomedical Materials*, vol. 15, 59–69, **2012**.
- [20] Bansiddhi, A. and Dunand, D. C., Shape-memory NiTi foams produced by replication of NaCl space-holders, *Acta Biomaterialia*, vol. 4, no. 6, 1996–2007, **2008**.
- [21] Li, D. S., Zhang, Y. P., Eggeler, G., and Zhang, X. P., High porosity and high-strength porous NiTi shape memory alloys with controllable pore characteristics, *Journal of Alloys and Compounds*, vol. 470, no. 1–2, 5–9, **2009**.
- [22] Zhang, Y. P., Yuan, B., Zeng, M. Q., Chung, C. Y., and Zhang, X. P., High porosity and large pore size shape memory alloys fabricated by using pore-forming agent (NH₄HCO₃) and capsule-free hot isostatic pressing, *Journal of Materials Processing Technology*, vol. 192–193, 439–442, **2007**.
- [23] Banhart, J., Manufacture, characterisation and application of cellular metals and metal foams, *Progress in Materials Science*, vol. 46, no. 6, 559–632, **2001**.
- [24] Li, B. Y., Rong, L. J., Li, Y. Y., and Gjunter, V. E., Synthesis of porous Ni-Ti shape-memory alloys by self-propagating high-temperature synthesis: Reaction mechanism and anisotropy in pore structure, *Acta Materialia*, vol. 48, no. 15, 3895–3904, **2000**.
- [25] Ryan, G., Pandit, A., and Apatsidis, D. P., Fabrication methods of porous metals for use in orthopaedic applications, *Biomaterials*, vol. 27, no. 13, 2651–2670, **2006**.
- [26] Chu, C. L., Chung, C. Y., Lin, P. H., and Wang, S. D., Fabrication and properties of porous NiTi shape memory alloys for heavy load-bearing medical applications, *Journal of Materials Processing Technology*, vol. 169, no. 1, 103–107, **2005**.
- [27] Chung, C. ., Chu, C. ., and Wang, S. ., Porous TiNi shape memory alloy with high strength fabricated by self-propagating high-temperature synthesis, *Materials Letters*, vol. 58, no. 11, 1683–1686, **2004**.
- [28] Goh, C. W., Gu, Y. W., Lim, C. S., and Tay, B. Y., Influence of nanocrystalline Ni-Ti reaction agent on self-propagating high-temperature synthesized porous NiTi, *Intermetallics*, vol. 15, no. 4, 461–467, **2007**.

- [29] Yuan, B., Zhang, X. P., Chung, C. Y., Zeng, M. Q., and Zhu, M., A Comparative Study of the Porous TiNi Shape-Memory Alloys Fabricated by Three Different Processes, *Metallurgical and Materials Transactions A*, vol. 37, no. March, 755–761, **2006**.
- [30] Greiner, C., Oppenheimer, S. M., and Dunand, D. C., High strength, low stiffness, porous NiTi with superelastic properties, *Acta Biomaterialia*, vol. 1, no. 6, 705–716, **2005**.
- [31] Lagoudas, Dimitris C., Vandygriff, Eric L., Processing and Characterization of NiTi Porous SMA by Elevated Pressure Sintering-Not Use, *Journal of Intelligent Material Systems and Structures*, vol. 13, no. December, 837–850, **2002**.
- [32] Yuan, B., Chung, C. Y., Zhang, X. P., Zeng, M. Q., and Zhu, M., Control of porosity and superelasticity of porous NiTi shape memory alloys prepared by hot isostatic pressing, *Smart Materials and Structures*, vol. 14, no. 5, S201–S206, **2005**.
- [33] Esen, Z. and Bor, Ş., Processing of titanium foams using magnesium spacer particles, *Scripta Materialia*, vol. 56, no. 5, 341–344, **2007**.
- [34] Otsuka, K. and Shimizu, K., Pseudoelasticity and shape memory effects in alloys, *International Metals Reviews*, vol. 31, no. 1, 93–114, **1986**.
- [35] Fan, G., Chen, W., Yang, S., Zhu, J., Ren, X., and Otsuka, K., Origin of abnormal multi-stage martensitic transformation behavior in aged Ni-rich Ti-Ni shape memory alloys, *Acta Materialia*, vol. 52, no. 14, 4351–4362, **2004**.
- [36] Aydoğmuş, T., Bor, E. T., and Bor, Ş., Phase transformation behavior of porous TiNi alloys produced by powder metallurgy using magnesium as a space holder, *Metallurgical and Materials Transactions A: Physical Metallurgy and Materials Science*, vol. 42, no. 9, 2547–2555, **2011**.
- [37] Lippold, J. C., *Welding Metallurgy and Weldability*. John Wiley & sons Inc., **2015**.
- [38] Losertová, M., Štencek, M., Matýsek, D., Štefek, O., and Drápala, J., Microstructure evolution of heat treated NiTi alloys, *IOP Conference Series: Materials Science and Engineering*, vol. 266, no. 1, **2017**.
- [39] Eggeler, G., Hornbogen, E., Yawny, A., Heckmann, A., and Wagner, M., Structural and functional fatigue of NiTi shape memory alloys, *Materials Science and Engineering A*, vol. 378, no. 1–2 SPEC. ISS., 24–33, **2004**.
- [40] Liu, Y. and Galvin, S. P., Criteria for pseudoelasticity in near-equiatomic NiTi shape memory alloys, *Acta Materialia*, vol. 45, no. 11, 4431–4439, **1997**.

APPENDIX 1: Technical Drawing of the Specimen Holder



APPENDIX 2: Calculated Porosity Percentages by Image Analysis

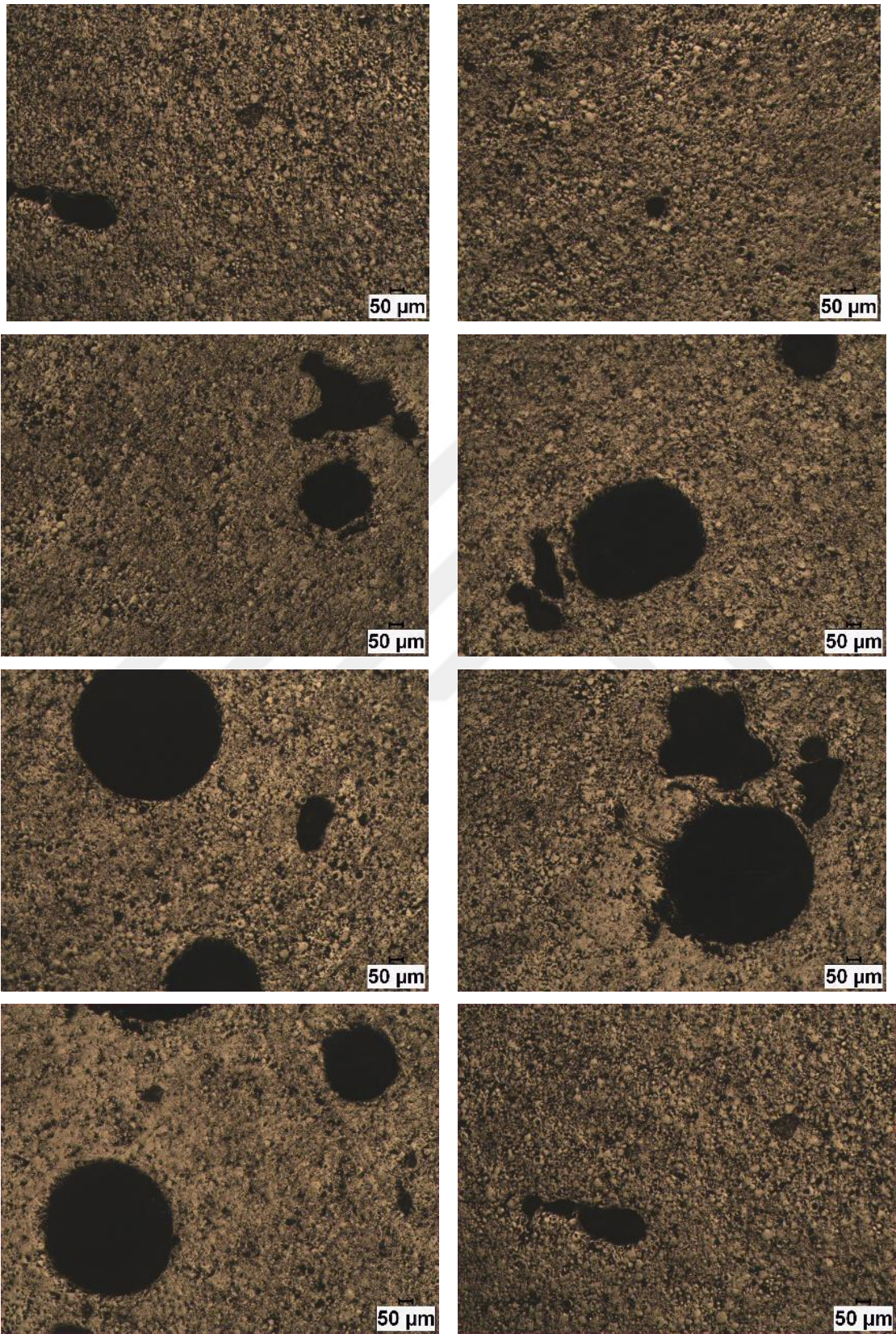
Image No	First 10% Mg Added Specimen	
	Calculated Percentage	Field Area
	(%)	(μm^2)
1	4.27	2,659,686.00
2	5.78	2,659,686.00
3	9.59	2,659,686.00
4	11.61	2,659,686.00
5	14.8	2,659,686.00
6	15.3	2,659,686.00
7	17.72	2,659,686.00
8	18.42	2,659,686.00
9	21.85	2,659,686.00
10	22.87	2,659,686.00
Average porosity level	14.2%	

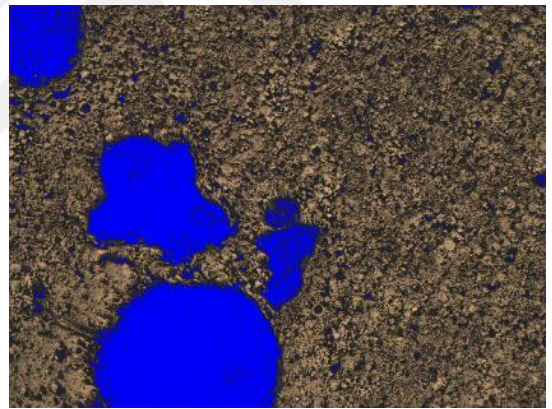
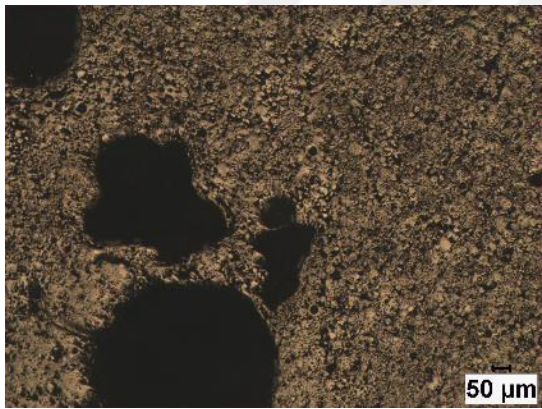
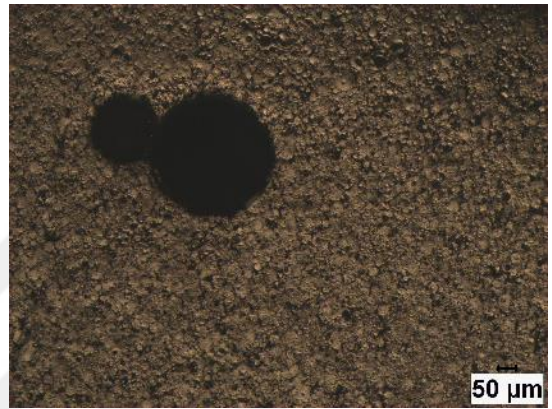
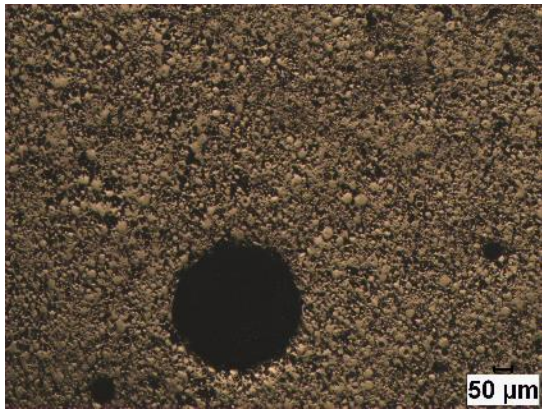
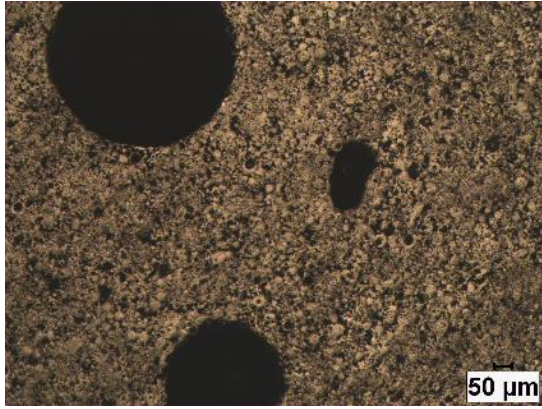
Image No	First 20% Mg Added Specimen	
	Calculated Percentage	Field Area
	(%)	(μm^2)
1	8.82	2,659,686.00
2	11.46	2,659,686.00
3	11.79	2,659,686.00
4	13.95	2,659,686.00
5	15.36	2,659,686.00
6	16.57	2,659,686.00
7	19.35	2,659,686.00
8	19.88	2,659,686.00
9	22.67	2,659,686.00
10	24.17	2,659,686.00
11	25.65	2,659,686.00
12	31.12	2,659,686.00
	33.76	2,659,686.00
Average porosity level	19.6%	

Image No	First 30% Mg Added Specimen	
	Calculated Percentage	Field Area
	(%)	(μm^2)
1	20.03	2,659,686.00
2	23.36	2,659,686.00
3	29.9	2,659,686.00
4	31.24	2,659,686.00
5	31.95	2,659,686.00
6	32.24	2,659,686.00
7	34.1	2,659,686.00
8	34.11	2,659,686.00
9	39.93	2,659,686.00
Average porosity level	30.8%	

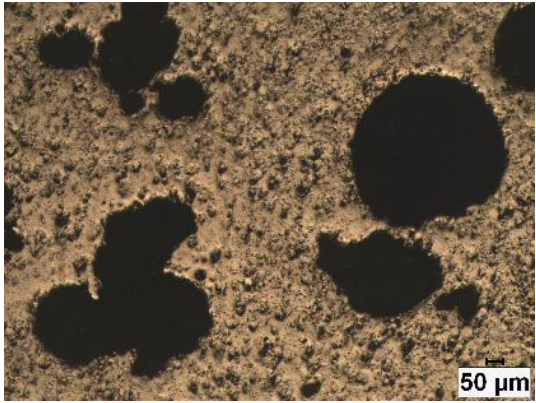
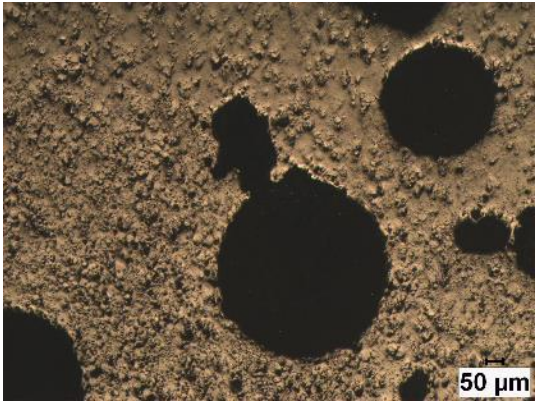
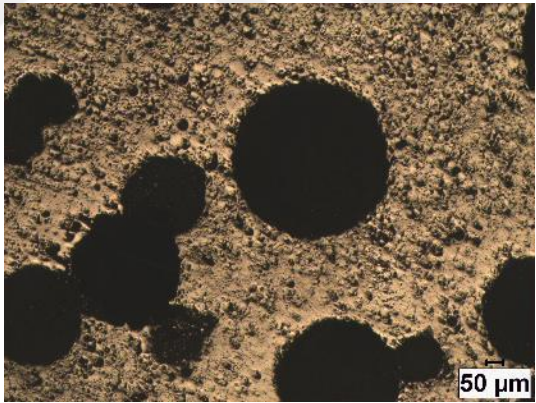
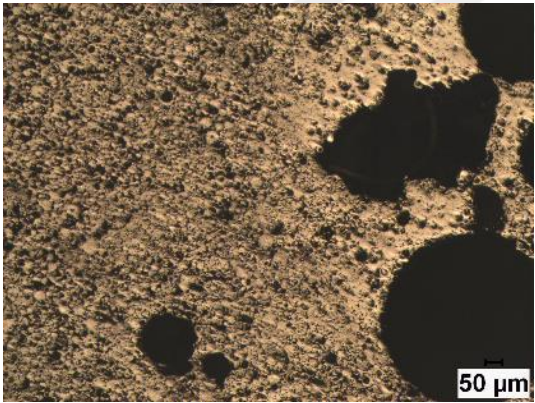
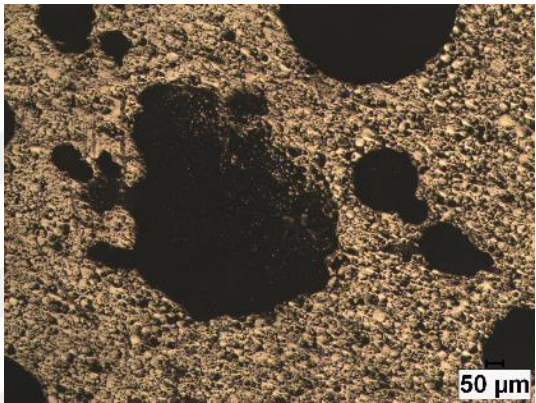
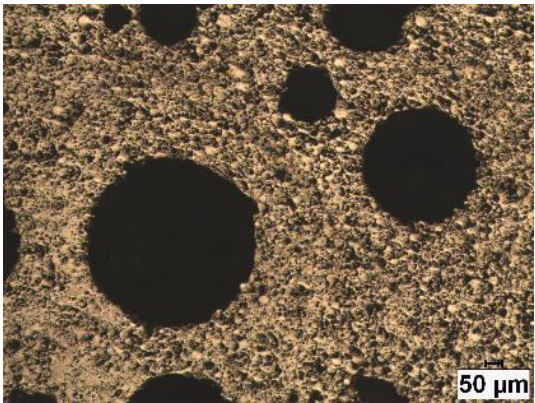
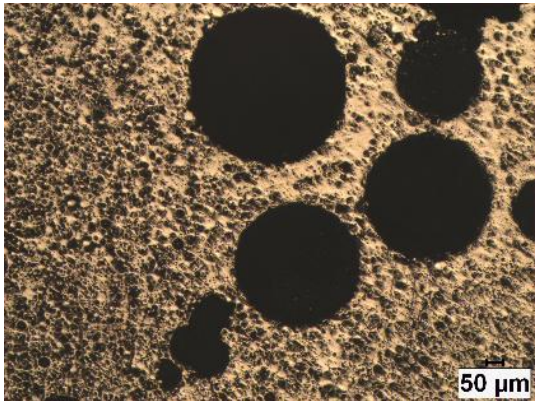
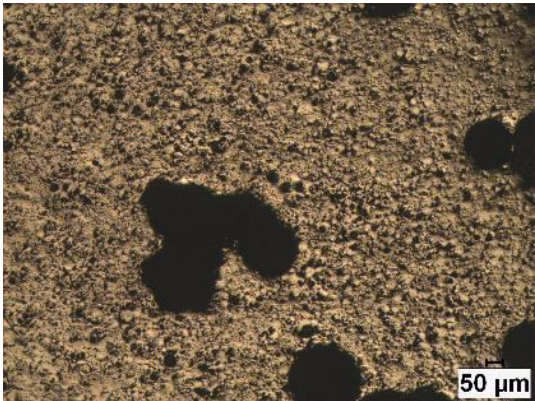
Image No	First 40% Mg Added Specimen	
	Calculated Percentage	Field Area
	(%)	(μm^2)
1	37.13	2,659,686.00
2	42.01	2,659,686.00
3	45.9	2,659,686.00
4	46.4	2,659,686.00
5	47.31	2,659,686.00
6	55.06	2,659,686.00
7	61.5	2,659,686.00
8	66.96	2,659,686.00
9	39.93	2,659,686.00
Average porosity level	50.3%	

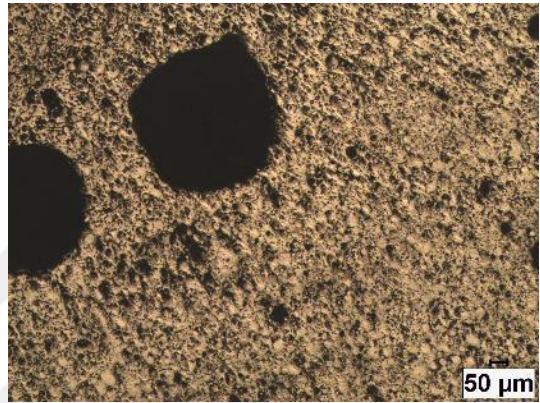
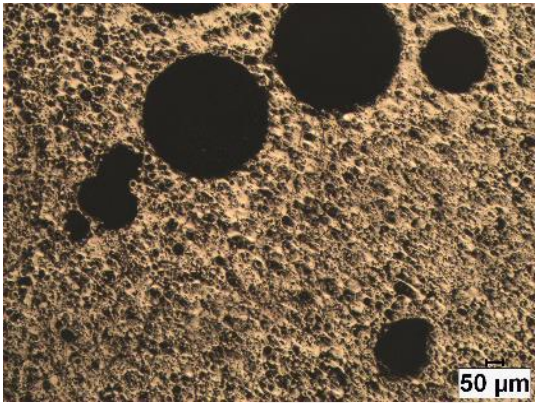
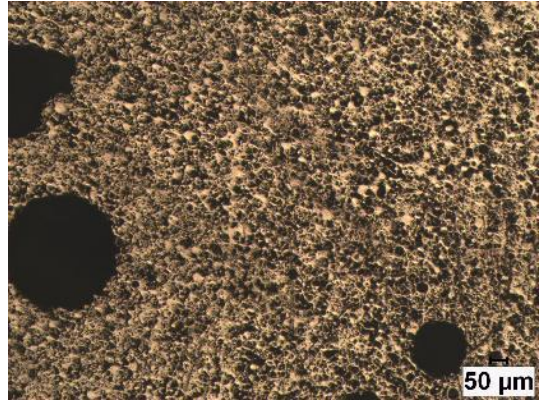
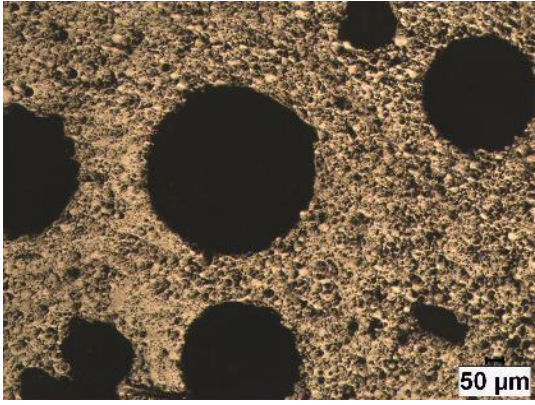
APPENDIX 3: Microscope Images of First 10% Mg Added Specimen



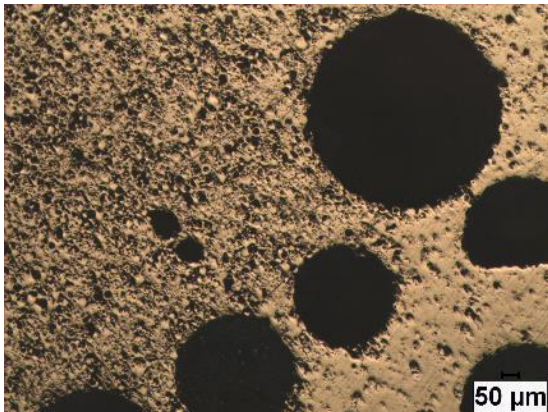
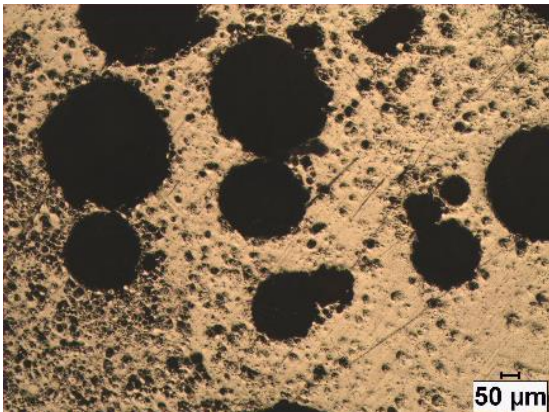
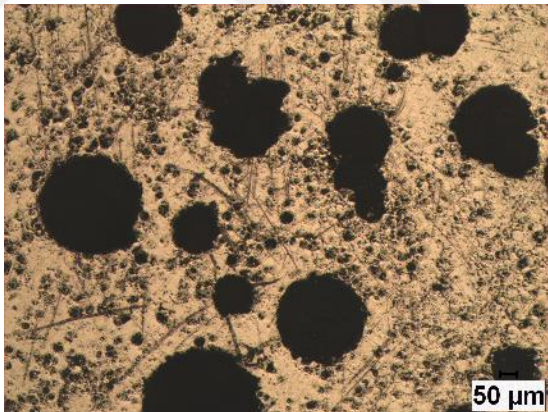
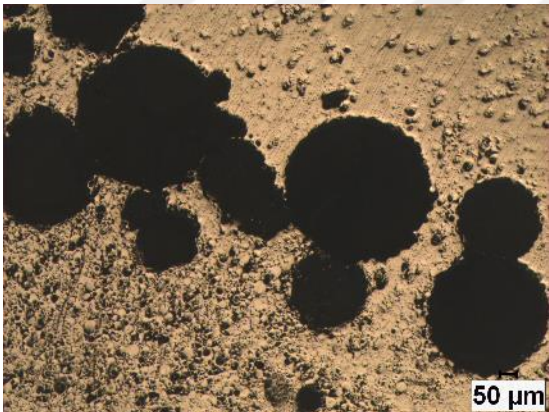
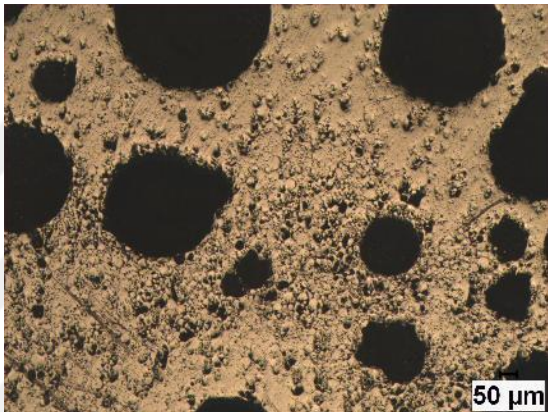
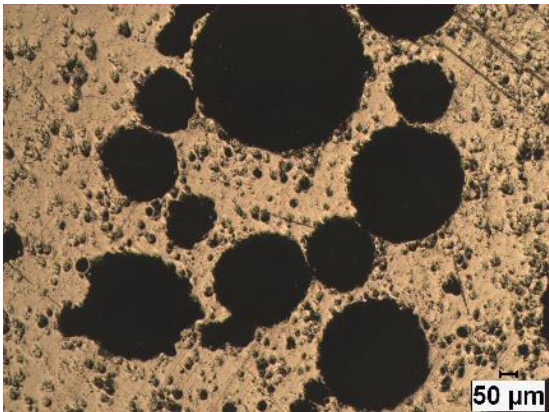
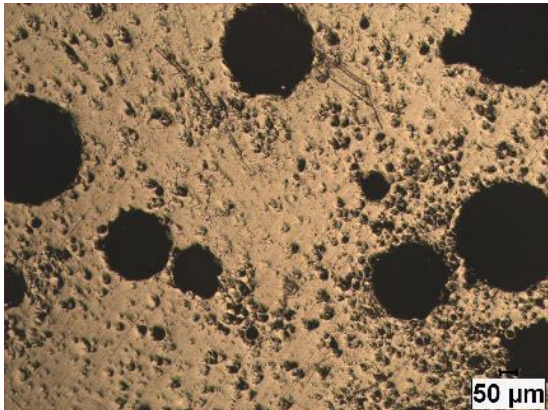
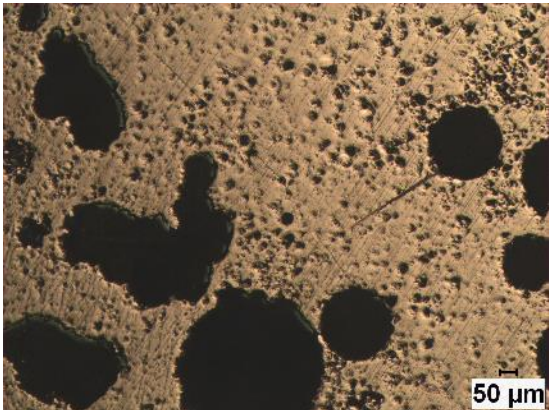


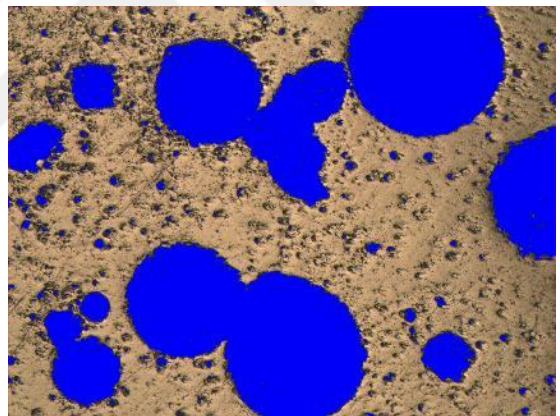
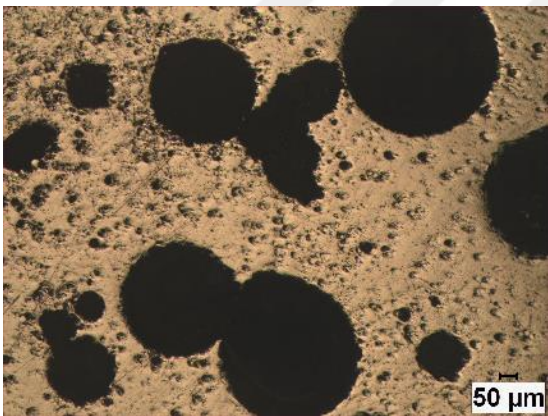
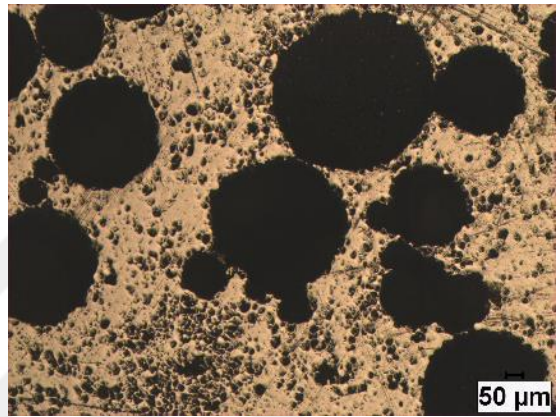
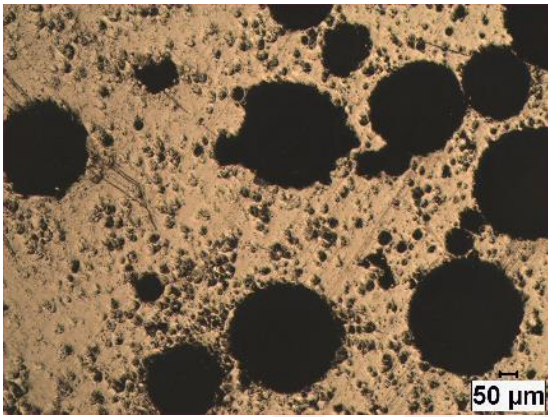
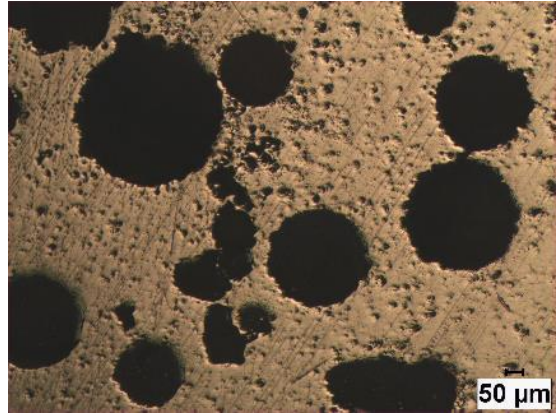
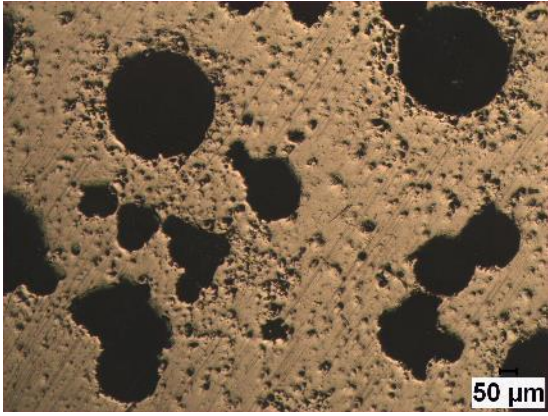
APPENDIX 4: Microscope Images of First 20% Mg Added Specimen



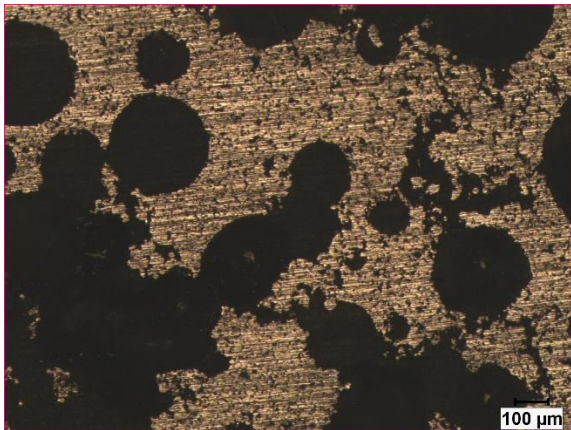
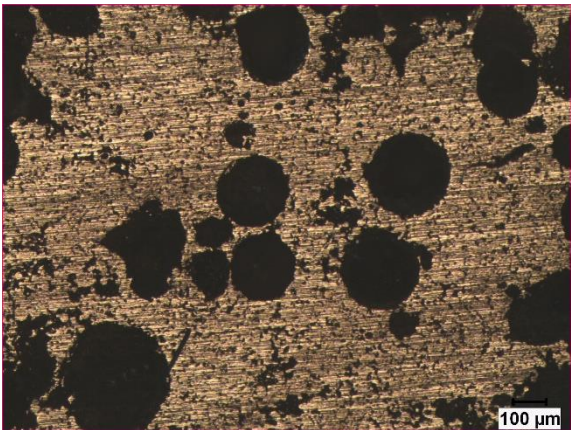
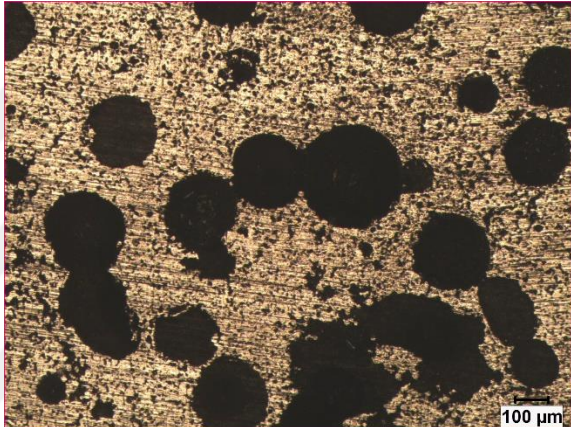
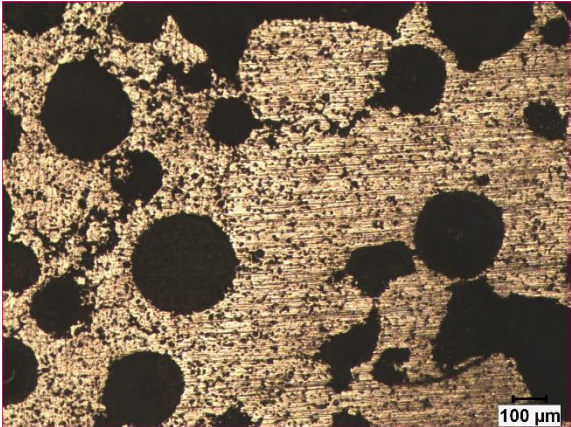
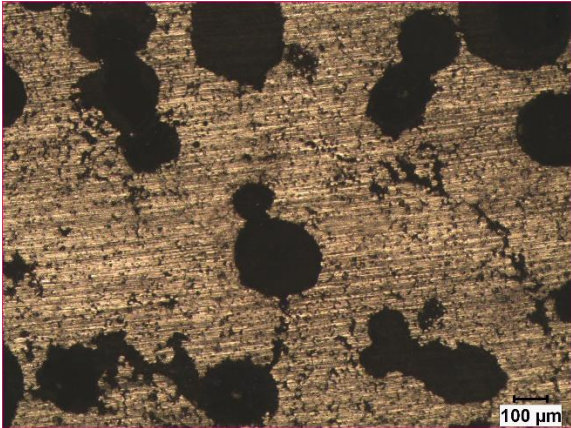


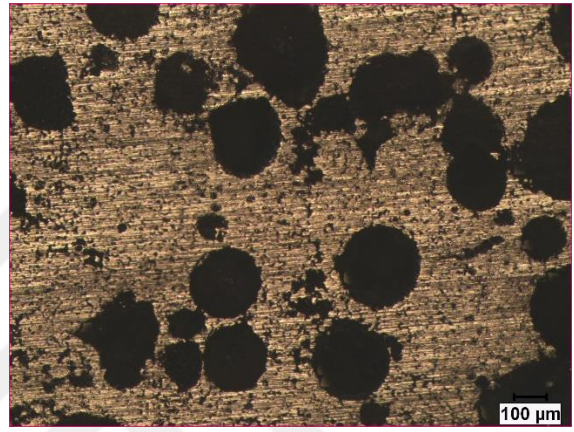
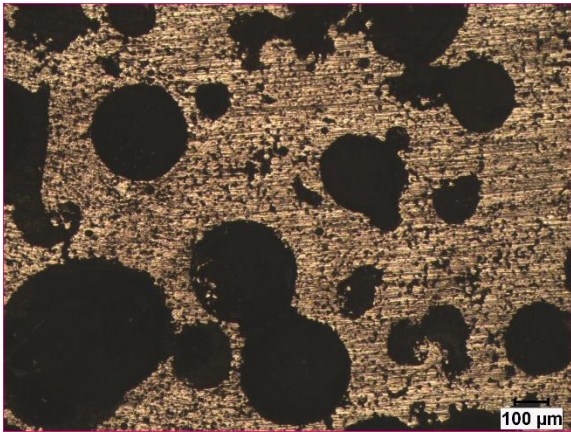
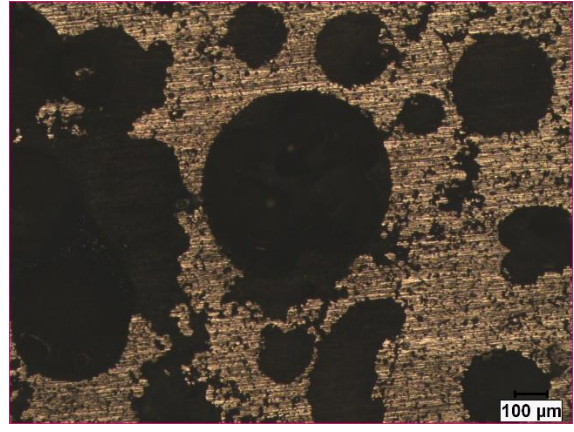
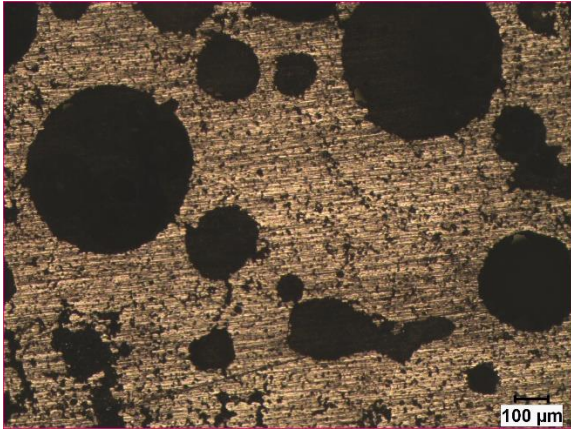
APPENDIX 5: Microscope Images of First 30% Mg Added Specimen





APPENDIX 5: Microscope Images of First 40% Mg Added Specimen





CURRICULUM VITAE

Credentials

Name, Surname : Gülfem, İnaner
Place of birth : İzmir
Marital Status : Single
E-mail : gulfem.inaner@gmail.com
Address :1550/1. Cad. Orta Doğu Çamlık Sitesi No:33/8 Ankara

Education

BSc. : Middle East Technical University, Mechanical Engineering, 2012

Foreign Languages

English – Advanced

Work Experience

Ekodenge AS: 2013 – Now

Areas of Experiences

Energy Conversion Systems, Heat Transfer, Advanced Materials and Composites

Projects and Budgets

Publications

Oral and Poster Presentations

“The Influence of Porosity Percentage on the Plateau Region of Pseudoelasticity Curves of Sintered Ni-Rich Niti Alloy”, ESOMAT, Antwerp, Belgium, 2015.



HACETTEPE UNIVERSITY
GRADUATE SCHOOL OF SCIENCE AND ENGINEERING
THESIS/DISSERTATION ORIGINALITY REPORT

HACETTEPE UNIVERSITY
GRADUATE SCHOOL OF SCIENCE AND ENGINEERING
TO THE DEPARTMENT OF MECHANICAL ENGINEERING

Date: 03/09/2018

Thesis Title / Topic: **DETERMINATION OF STRESS VS. TEMPERATURE PHASE DIAGRAM OF NITI SHAPE MEMORY ALLOYS WITH DIFFERENT POROSITY LEVELS**

According to the originality report obtained by ~~myself~~/my thesis advisor by using the *Turnitin* plagiarism detection software and by applying the filtering options stated below on **03/09/2018** for the total of **58** pages including the a) Title Page, b) Introduction, c) Main Chapters, d) Conclusion sections of my thesis entitled as above, the similarity index of my thesis is **5 %**.

Filtering options applied:

1. Bibliography/Works Cited excluded
2. Quotes excluded / ~~included~~
3. Match size up to 5 words excluded

I declare that I have carefully read Hacettepe University Graduate School of Science and Engineering Guidelines for Obtaining and Using Thesis Originality Reports; that according to the maximum similarity index values specified in the Guidelines, my thesis does not include any form of plagiarism; that in any future detection of possible infringement of the regulations I accept all legal responsibility; and that all the information I have provided is correct to the best of my knowledge.

I respectfully submit this for approval.

18.09.2018

Date and Signature

Name Surname: GÜLFEM İNANER

Student No: N13224858

Department: MECHANICAL ENGINEERING DEPARTMENT

Program: MECHANICAL ENGINEERING DEPARTMENT

Status: Masters Ph.D. Integrated Ph.D.

ADVISOR APPROVAL

APPROVED.

ASSOC. PROF. DR. BENAT KOÇKAR

(Title, Name Surname, Signature)